Synthesis and Characterization of Flat Sheet and Hollow Fiber Membranes for Filtration of Uremic Toxins in Dialysate

Rachel Xiaoyu Shi

A thesis

submitted in partial fulfillment of the

requirements for the degree of

Master of Science

University of Washington

2023

Committee:

Buddy D. Ratner

Bruce J. Hinds

Program Authorized to Offer Degree:

Department of Bioengineering

University of Washington

Abstract

Synthesis and Characterization of Flat Sheet and Hollow Fiber Membranes for Filtration of Uremic Toxins in Dialysate

Rachel Xiaoyu Shi

Chair of the Supervisory Committee:

Buddy D. Ratner

Department of Bioengineering

End-stage renal disease (ESRD) is a highly prevalent disease affecting around 750k people in the United States alone. With over 60% of ESRD patients receiving hemodialysis, it remains the most common form of treatment. However, traditional hemodialysis restricts the lives of patients, necessitating frequent long sessions at dialysis clinics, while having a poor prognosis with a 42% 5-year survival rate. Portable dialysis systems are a solution which can provide continuous dialysis and promote patient autonomy. One major challenge for portable dialysis is the high volumes of dialysate consumed; 120 L of dialysate is needed for one hemodialysis session. To circumvent this challenge, we investigated polymeric materials for the continuous filtration of toxins out of a small volume of dialysate: a dialysate recycling system. Electrodecomposition is a method to remove urea from dialysate but is disrupted by the presence of glucose. Thus, we aimed to harness polymeric materials for size-exclusion filtration for the

separation of urea and glucose. By analyzing the effect of polymer type, concentration, additives, thermal annealing, and synthesis temperature on membrane formation, we developed and optimized a cellulose acetate flat sheet membrane with a urea to glucose separation ratio of over 30. We then synthesized and analyzed the formation mechanisms of hollow fiber membranes with different polymer types, given their superior surface area to volume ratio compared to flat sheet membranes. We found that polyethersulfone membranes demonstrated specific qualities promising for dialysate filtration applications, such as multiple skin layers, polymer chain reorientation, and well-formed channeled macrovoids. These findings elucidate the mechanisms of polymer material formation while providing synthesis techniques for successful materials that can be incorporated into a dialysate recycling system in the future.

Acknowledgements

Firstly, I would like to express my gratitude and thanks to my supervisor, Professor Buddy D. Ratner. Your invaluable guidance throughout the past three years has been instrumental for my growth as an undergraduate and graduate researcher. I am truly thankful for the opportunities you have provided and your support in all facets of my academic career, whether it is presenting at conferences, drafting patents, or simply troubleshooting experiments. Your wisdom and dedication to the field will continue to inspire me in all my future endeavors.

I would like to thank Professor Bruce Hinds, my committee member, for providing his expertise throughout my thesis and for his inspiring achievements towards portable dialysis that fueled my passion for my research project.

Thank you to my parents, grandparents, and sister for always providing a warm and loving environment to which I can return after long days at school, work, or the lab. I will eternally be grateful for the warm meals and long drives.

To my partner Carter: thank you for always being in my corner, no matter the circumstances or distance. You motivate me to be a better student, researcher, and person. Your love and support is so incredibly meaningful to me.

To my closest friends Daniel and Tiara: thank you for sticking with me through thick and thin. I cannot imagine where I would be today if I hadn't met you all six years ago. I hope to have many more spontaneous food trips and midnight phone calls with you.

Thank you to Dr. Runbang Tang, my mentor throughout my Bachelor's, for guiding me when I was a fledgling student researcher finding my way in the lab.

Thanks also to all the members of the Ratner Lab (past and present) and collaborators that have walked alongside me in this journey. You have provided an incredible community as fellow researchers and friends.

Finally, I wish to acknowledge the University of Washington for providing me with educational resources for the past six years, throughout which I completed Transition School under the Robinson Center for Young Scholars (2017-2018), my Bachelor of Science in Bioengineering (2018-2022), and now my Master of Science in Bioengineering (2022-2023).

Table of Contents

Chapter 1: Introduction

1.1 Kidney Failure and Treatment

Chronic kidney disease (CKD) affects over 15% of the U.S. population and 9% of people worldwide (Cockwell & Fisher, 2020; Centers for Disease Control and Prevention, 2021). CKD patients suffer from any degree of reduced kidney function, with the formal diagnosis being determined after a patient exhibits evidence of kidney damage over a three-month period through estimated glomerular filtration rate (eGFR) and albumin concentration measurements (Arora, 2021; Matovinovic, 2009). Though eGFR varied based on factors such as age, sex, body type, and race, an eGFR below 60 or high levels of albumin in urine is indicative of loss of kidney function. CKD patients are more susceptible to complications such as cardiovascular disease, anemia, malnutrition, and depression (Shaikh, Hashmi, & Aeddula, 2023).

Many CKD patients experience progressive decline of kidney function, with 50% developing end-stage renal disease (ESRD) within ten years (Cerqueira, et al., 2014). In the U.S., ESRD affects approximately 750,000 people, with this number continuing to rise annually (Saran, et al., 2020). Patients with ESRD have a significantly reduced glomerular filtration rate of <30 mL/min, increasing vulnerability to the aforementioned CKD complications through fluid retention, reduced erythropoietin synthesis, and altered bone/mineral metabolism (Abbasi, 2010). ESRD patients no longer have kidneys capable of performing standard blood filtration and thus cannot excrete wastes and excess fluid. Therefore, ESRD requires direct medical intervention, as patients generally only survive for a couple of days or weeks without treatment. Even with treatment, the life expectancy of ESRD patients can be as low as five years.

The quality of life for ESRD patients is significantly reduced. In addition to the comorbidities associated with CKD, ESRD patients may experience nausea, vomiting, loss of appetite, and fatigue (Mayo Clinic, n.d.). Kidney disease is associated with high financial burden. The associated annual Medicare expenditure for CKD patients is around $84 billion, and the associated annual Medicare expenditure for ESRD patients specifically is around $36 billion; combined, the expenditure is upwards of $120 million (Saran, et al., 2020). In addition, kidney failure disproportionately affects minority and low-income populations. In the U.S., this includes African Americans, Native Americans, and Hispanics (United States Renal Data System, 2018). The combination of high treatment costs and low-income populations being disproportionately affected leads to poor health outcomes.

The current treatments for ESRD are kidney transplantation and dialysis. The former is severely limited by the availability of donor organs and requires a lengthy donor match and surgery process, with a median wait time of 3.6 years for a first kidney transplant (United States Renal Data System, 2018). After surgery, patients are placed on a lifetime regimen of immunosuppressants with an undesirably high rate of kidney transplant failure (Perl, 2014). Treatment with dialysis is more common, as dialysis is more accessible and can serve as a substitute treatment for patients after kidney transplant failure.

Hemodialysis, a specific form of dialysis in which a dialyzer machine is used to filter blood that is then returned to the body, was invented in the 1940s and remains as the most common treatment for ESRD patients (Blagg, 2007). Despite 63.2% of ESRD patients undergoing hemodialysis, it remains roughly unchanged since its conception and is not comparable to the function of a healthy human kidney (United States Renal Data System, 2018). The prognosis for hemodialysis patients is grim at a 42% five-year survival rate, with the large fluid and electrolyte

shifts that occur during hemodialysis correlating with sudden death (Bleyer, et al., 2006). Hemodialysis is reliant on machinery that can generally only be accessed in dialysis clinics. Treatment is conducted in three-to-five-hour sessions, three times a week. Therefore, toxins in the blood are only eliminated intermittently and accumulate between sessions. Not only is this technique suboptimal compared to healthy kidneys that continuously filter blood, but the strict hemodialysis schedule is also inconvenient and exhausting, reducing patient adherence to treatment. Recent efforts to improve dialysis patients' health, well-being, and freedom have led to the development of portable dialysis devices.

In addition to providing greater flexibility in patient lives, portable dialysis devices also enable continuous dialysis. Frequent hemodialysis sessions have been shown to lead to faster decline of kidney function (Chertow, 2010; Daugirdas, 2013). Thus, by providing continuous dialysis similar to a healthy human kidney, portable dialysis has the potential to improve patient outcomes. However, a major hurdle for portable dialysis is the large volume of dialysate fluid needed. In traditional hemodialysis, approximately 120 L of dialysate is needed to clear a baseline of ~240 mmol (14 g) of urea from the bloodstream, making fresh dialysate sourcing and storage a significant challenge (Van Gelder, 2020). Because portable dialysis can only accommodate up to 500 mL of dialysate, purification units are necessary to create a continuous dialysate regeneration system.

1.2 Developments in Portable Dialysis

Existing dialysate purification systems harness absorbents such as activated carbon and zeolites, which are heavy and require frequent replacement. For example, the portable dialysis system ViWAK PD (Vicenza wearable artificial kidney for peritoneal dialysis) consisted of a dual lumen peritoneal catheter and a circuit for dialysate regeneration via sorbent-based filtration

(Claudio Ronco, 2007). Although the system successfully removed large proteins such as β2-MG and angiogenin, it required a complex mixture of sorbents to remove smaller molecules such as urea. Furthermore, the patient would still be required to perform two peritoneal dialysis exchanges per day and there were significant costs associated with the daily replacement of sorbent filters. Other devices include the wearable artificial kidney (WAK), which generates dialysate flow across a dialyzer membrane, followed by sorbents and urease (Van Gelder, 2020). Notably, the dialysate travels through activated microporous carbon sorbent, urease sorbent, zirconium sorbent, and a bicarbonate/electrolyte pump before it is suitable for use. Limitations in this case are that sorbents are heavy and require frequent replacement, which can impose additional physical and financial burdens on patients and their families.

Recently, electro-decomposition has been developed as an alternative method of purifying dialysate that is inexpensive and durable. Researchers under the Center for Dialysis Innovation have developed a novel TiO2 nanowire photoelectrochemical system for decomposition of urea, the waste solute with the highest daily molar production rate, into N2 and CO2 (Fig. 1) (Shao, 2019). This system addresses some of the major shortcomings of sorbents such as activated carbon, which has low affinity for urea. Despite this advancement, the system requires optimization for compactness and energy efficiency. Urea degradation is inhibited by the presence of glucose because glucose is thermodynamically favored for decomposition over urea. A highly-concentrated dialysate solution may contain 70 to 130 mg/dL of glucose (Baura, Medical device technologies: A systems based overview using engineering standards (Second ed.), 2021). Not only is this energy-inefficient, glucose

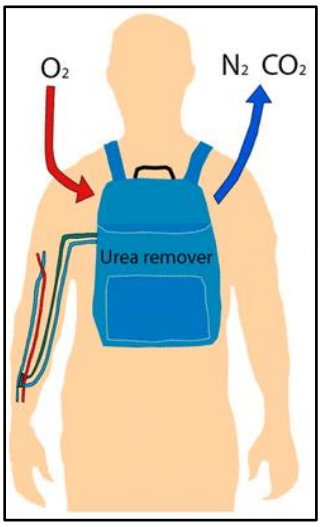

Fig. 1. Portable dialysis urea removal schematic (Shao, 2019).

decomposition generates several byproducts, including peroxides and glucaric acids. Thus, in order to engineer a device with sufficient capacity for dialysate regeneration, it is important to separate glucose and urea in dialysate before the electro-decomposition step.

1.3 Flat Sheet Membranes

Flat sheet polymeric membranes have traditionally been used in a variety of applications, including food industries, gas separation, pharmaceutical industries, water desalination, energy generation, and wastewater treatment (Vatanpour, 2022). Flat sheet membranes use a single-layer configuration, in which feed solution is flowed to one side and permeated solution collected on the other side (Imemflo, 2023). The two primary ways of utilizing flat sheet membranes are dead-end and cross-flow configurations. In dead-end filtration, the feed solution is sent perpendicularly through the membrane. In cross-flow filtration, there is a flow tangent to the membrane surface. They can be tuned for a wide range of solute separations and are typically classified into four categories: microfiltration, ultrafiltration, nanofiltration, and reverse osmosis (organized by decreasing pore size) (Gwak, 2018).

Briefly, microfiltration membranes have a pore size of 0.1 – 0.5 μm and are used to filter out contaminants such as bacteria, cells, and dust (FreePurity, n.d.). Ultrafiltration membranes have pore sizes of 0.01 – 0.1 μm. They require a higher osmotic pressure and are used to filter out silica, viruses, endotoxins, and proteins. Ultrafiltration is conventionally used for blood filtration in dialysis. Nanofiltration membranes have pore sizes of 0.001 – 0.01 μm, filtering salts, dyes, and sugars. Finally, reverse osmosis membranes have a pore size range of 0.0001 μm – 0.001 μm. Their small pore size allows for removal of ions for desalination purposes, with a high osmotic pressure needed for filtration and lower flowrate on the order of gallons per day.

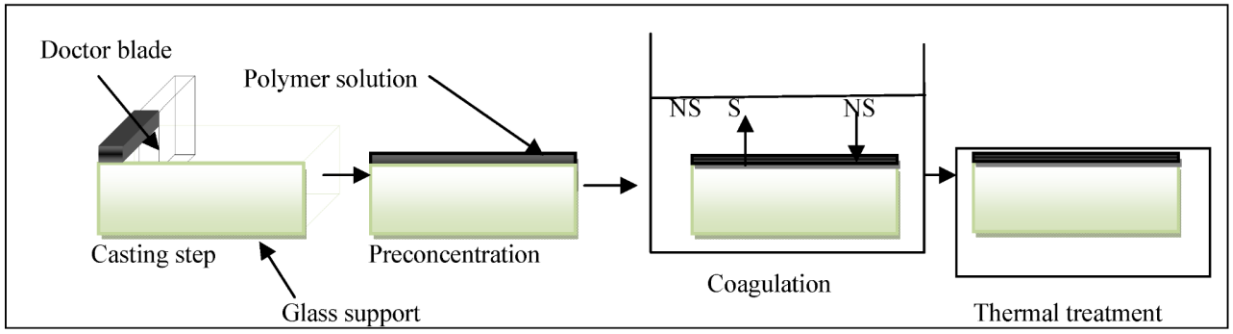

Figure 2. Schematic of membrane preparation via the immersion precipitation/phase inversion method (El-Gendi, 2007).

Immersion precipitation is one of the most common methods for flat sheet membrane synthesis, in which a thin film of a concentrated polymer dope solution is cast onto a glass support and immersed in a bath of nonsolvent (Fig. 2) (El-Gendi, 2007). The membrane forms due to the exchange of solvent (from the polymer solution) and nonsolvent (from the bath). Notably, this method creates pores within the polymer matrix, which give the membrane its filtration properties. After membrane formation, there is another optional step to thermally treat the membrane by immersing it in a hot nonsolvent bath. Throughout the synthesis process, parameters such as casting thickness, casting temperature, coagulation bath temperature, and heat treatment temperature influence the morphology and performance of the resulting membrane.

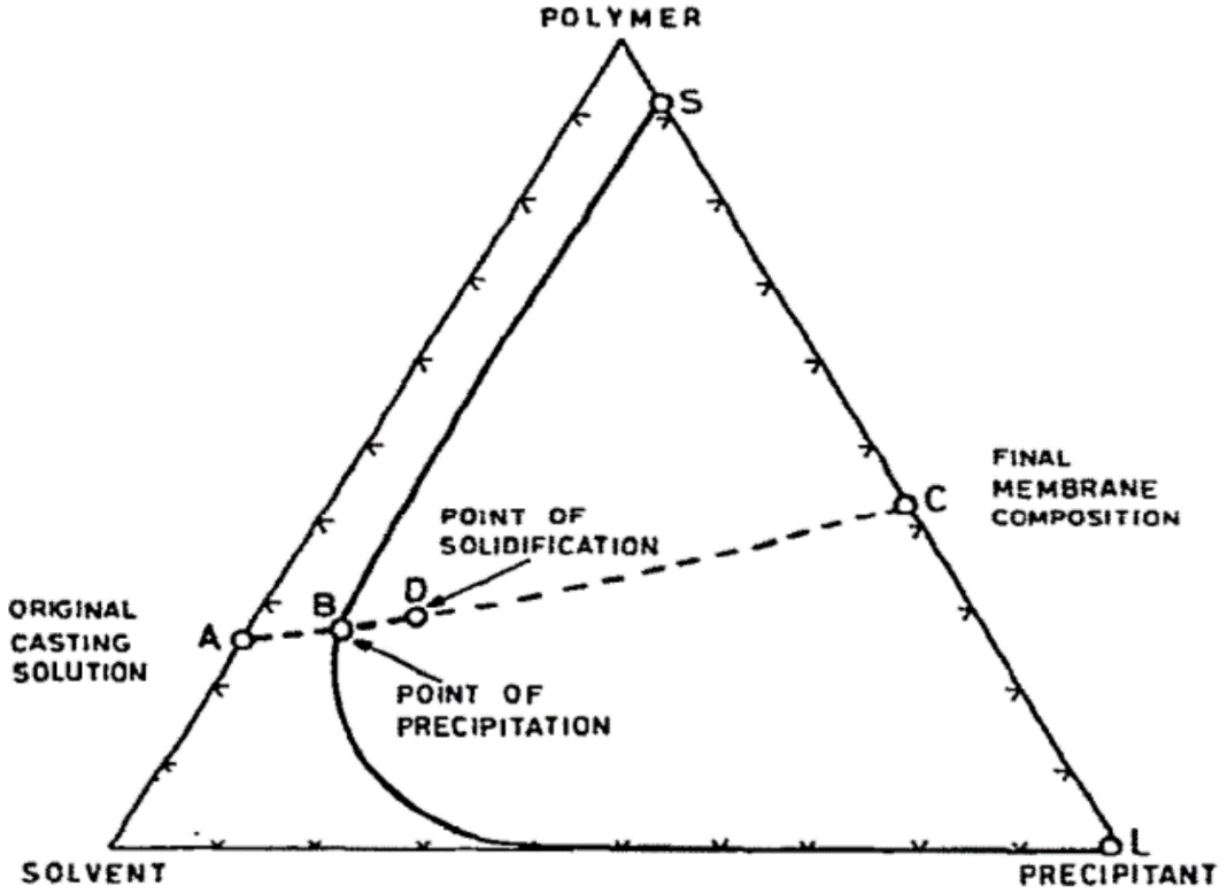

Figure 3. Schematic phase diagram of the polymer/solvent/nonsolvent system demonstrating the thermodynamics of immersion precipitation (Strathmann, 1977).

The thermodynamics of immersion precipitation can be captured by a ternary polymer/solvent/nonsolvent phase diagram, which is valid at constant temperature and pressure (Fig. 3) (Holda A. V., 2015; Idris, 2017; Strathmann, 1977). Membrane formation begins at point A, which represents the original casting solution consisting solely of polymer and solvent. During membrane formation, the system separates into a polymer-rich mostly solid phase and a polymer-poor mostly liquid phase (solid line). At point C, we have the final membrane composition. Point C represents the overall porosity of the membrane consisting of the polymer-rich phase (membrane structure, point S) and polymer-poor phase (pores filled with nonsolvent, point L). Examining the trajectory of immersion precipitation, solvent-nonsolvent exchange occurs after immersion into a

nonsolvent bath and is represented by the dashed line in Fig. 3. Point B is the point at which the polymer first begins to precipitate out of solution. As we progress along the dashed trajectory, the viscosity of the polymer-rich phase increases. At point D, the polymer is considered to be a solid due to its very high viscosity and limited bulk movement. As more solvent-nonsolvent exchange occurs, we observe shrinkage of the polymer-rich phase. Given these insights on the process of membrane formation, it is important to examine the governing parameters that determine the trajectory and characteristics of the final membrane.

Studies on the filtration capabilities of polymeric membranes have found that molecular weight, geometry, dipole, and membrane charge are determinants of the retention of specific organic molecules. The type of polymer dissolved into the dope solution is one such important factor. In general, the polymer selected should be soluble in an organic solvent with very minimal solubility in water (Baker, 1999). They are typically amorphous with a molecular weight of 30,000-40,000 Da. Protease ultrafiltration and aerosol filtration have been characterized with dope solutions consisting of 10-20 wt% polysulfone (PSF) and polyethersulfone (PES) dissolved in n-methyl-2-pyrrolidone (NMP) (Ali, 2012; Huang, 2006). Higher PSF/PES concentrations were found to shrink pore sizes, decreasing overall flux through the membrane and increasing the protease rejection rate. Polyimides (PI) are also a viable candidate for the polymer base of membranes. Membranes synthesized from dope solutions of PI in NMP, dimethylformamide (DMF), dimethyl sulfoxide (DMSO), or dimethylacetamide (DMAc) are stable in harsh polar aprotic solvent environments and demonstrate good solute separation performance (Toh, 2007). Lastly, cellulose acetate membranes are of interest since cellulose acetate is neutral, inexpensive, and synthesized from cellulose, a renewable source (Ruggiero, 2015). Modulation of cellulose

acetate membrane porosity has been achieved by including additive compounds in the polymer solution due to reorganization of matrix structure during membrane formation (Fornazier, 2021).

The presence and species of additives added into the dope solution influences the properties of the synthesized membrane, as additives may change the chemical interactions within the polymer/solvent/nonsolvent system as well as the thermodynamics of membrane formation by affecting viscosity. Addition of 1,4-dioxane into a PI-based dope solution resulted in the formation of membranes with smaller pores and higher solute rejection (Soroko, 2011). Similarly, adding 1% magnesium perchlorate led to membranes with decreased pore size. A study specifically evaluating alcohol additives for PES found that water permeation increased with greater n-propanol concentration in the casting solution (Saleh, 2009). Poly(vinyl pyrrolidone) (PVP) is a popular additive that has been shown to produce membranes with higher porosity at specific concentrations. 0-3 wt% PVP enhanced macrovoid formation and water permeation in cellulose acetate membranes but increasing the concentration to 3-6 wt% reduced macrovoid formation and reduced permeation (Salijoughi, 2009).

An additional factor in the synthesis process of immersion precipitation membranes is the choice of solvent, which has been demonstrated to affect permeability and selectivity properties. NMP has been theorized to be a suitable solvent for PSF due to the low relative energy difference between NMP and PSF. However, the relative energy difference between polymer and solvent does not necessarily correlate with membrane performance, as Chakrabarty et al. identified that using DMAc rather than NMP resulted in greater selectivity (Chakrabarty, 2008). Generally, a suitable organic solvent should be able to fully dissolve the polymer of choice. Additionally, if the solvent is highly miscible with the nonsolvent, the membrane will be more porous. If the solvent and nonsolvent are not miscible, the membrane will be denser.

Synthesis parameters related to procedure and setup are also important considerations. For example, increasing the evaporation time (time elapsed between casting the dope solution onto the glass support and immersing the support into the nonsolvent bath) resulted in a more concentrated layer at the top of the casted dope solution. After immersion, the layer became a barrier for solvent-nonsolvent exchange, reducing the rate of demixing and decreasing permeance through the synthesized membrane (Holda A. V., 2014). Other procedural parameters include the thickness of the casted film on the glass support and temperature of the nonsolvent bath, in which increasing the thickness of the casted film and lower nonsolvent bath temperature was found to increase gaseous flux but decrease selectivity when used to separate O_2 and N_2 (Madaeni, 2011).

1.4 Hollow Fiber Membranes

Hollow fibers (HF) membranes have recently become commercially available as an alternative geometry for standard flat sheet membranes. Like flat sheet membranes, they have applications across many industries, including wastewater treatment, desalination, gas separation, and pharmaceutical manufacturing (Imemflo, 2023; Kim, 2023; Sewerin, 2021). HF membranes have a higher surface area to volume ratio which are well suited for high capacity applications such as dialysis. In fact, modern dialyzers for blood filtration consist of hollow fibers compacted into a cartridge; globally, roughly 300 million HF hemodialyzers are used for 2.6 million ESRD patients per year (Ronco, Haemodialysis membranes, 2018).

HF filtration is typically conducted in one of two configurations (Imemflo, 2023). For inside-out configuration, feed solution is sent through the inside of the HFs and permeate is collected from the outside of the fibers, leaving the retentate in the HF lumens. For outside-in configuration, feed solution is sent external to the HFs and permeate is collected from the lumen of the fibers, leaving the retentate on the outside of the HFs. In modern hemodialysis, HFs are

utilized in the inside-out configuration for blood filtration, in which blood is flowed through the lumens of the fibers and dialysate is flowed countercurrent external to the fibers (Ji, 2023). The difference in solute concentration between the lumen and outside of the HFs drives diffusive-convective mass transfer.

HF membranes for dialysis are typically classified into cellulosic and synthetic groups (Ji, 2023). Cellulose-based HF membranes are structurally symmetric with the ability to remove small solutes. They have been fine-tuned since the 1980s to improve hemocompatibility and reduce complement activation through the alternative pathway (Kohlova, 2019). Cellulose triacetate hollow fiber membranes in particular are often used in modern hemodialyzers because they can be synthesized for low to ultra-high-flux performance for clearance of solutes of different molecular weights.

Synthetic HF membranes encompass membranes made out of materials such as PSF and PES (Ji, 2023). Early versions had a wall thickness of 100 μm, but modern reductions in thickness have made synthetic HFs suitable for high-flux filtration (Ronco, 2018). PSF and PES HF membranes have high chemical and thermal stability, enabling conventional sterilization techniques (Ji, 2023). In addition to their effectiveness at solute removal for a broad range of hemodialysis modalities, these qualities make PSF and PES HFs a promising candidate for further improvements in filtration.

HF membranes, regardless of the polymer base, are created through a process known as spinning (Ahmad, 2019). Spinning typically involves extrusion of a concentrated polymer dope solution through a spinneret, a device consisting of two or more concentric needles (Fig. 4). The polymer solution is composed of a particular polymer (e.g. cellulose acetate, PSF, PES) dissolved in organic solvent (e.g. NMP, dioxane). In standard HF production, polymer solution is extruded

in the outer needle and nonsolvent is extruded through the inner needle using gas extrusion or a pump. As the polymer solution and nonsolvent make contact, solvent-nonsolvent exchange occurs, allowing for phase inversion. The HF begins to take the form of a hollow cylinder as it solidifies, forming a porous matrix that facilitates high surface area filtration.

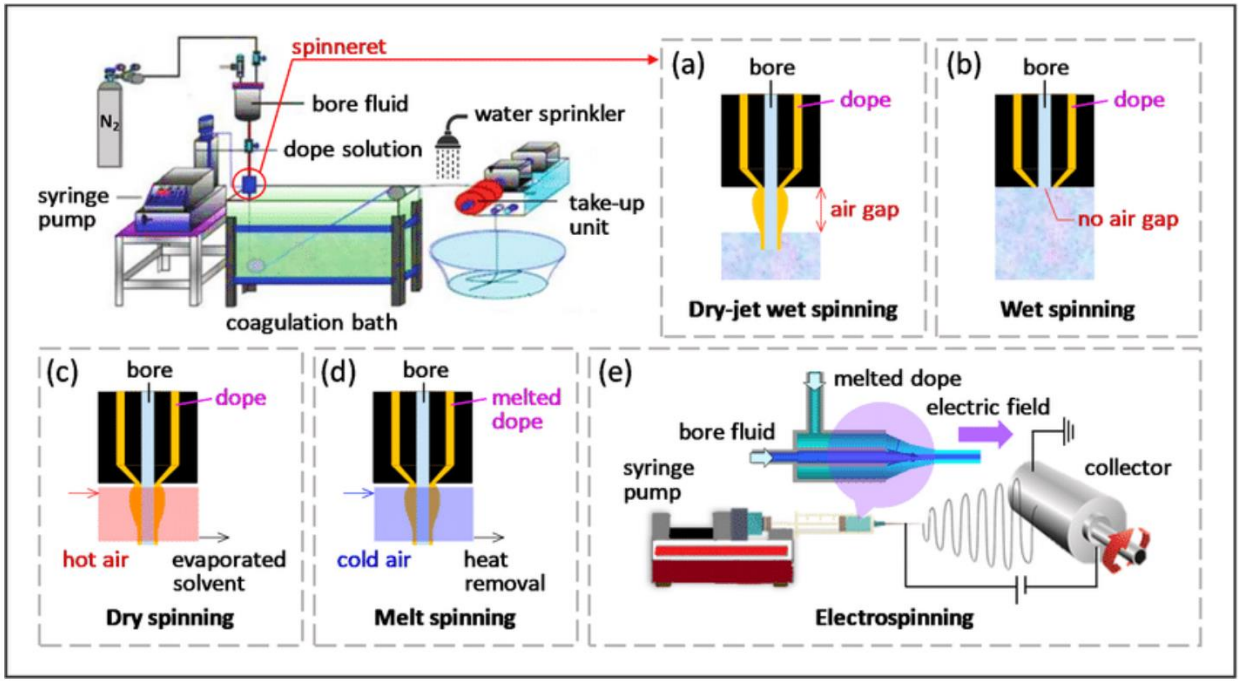

Fig. 4. Overview of common hollow fiber spinning techniques: (a) dry-jet wet spinning, (b) wet spinning, (c) dry spinning, (d) melt spinning), (e) electrospinning (Lau, 2022).

There are several common types of spinning: melt spinning, wet spinning, and dry-jet wet spinning (Fig. 4) (Ahmad, 2019). In melt spinning, polymer is melted in an extruder and travels through a spinneret with a specific cross section (Rwei, 2001; Ahmad, 2019). The subsequent melt stream is drawn and cooled after it exits the spinneret, forming a nascent filament that is taken up by a roller. Melt spinning is suitable for polymers with low melting points. Wet spinning and dry-jet wet spinning are considered under the same umbrella of solution spinning as they are similar in technique. In wet spinning, the concentrated polymer dope solution is extruded through the spinneret along with nonsolvent directly into a nonsolvent bath. At the interface of the polymer

solution and nonsolvent, solvent-nonsolvent exchange occurs and the fiber precipitates out of solution. During this solidification process, transfer of solvent and nonsolvent causes a membrane matrix consisting of voids and defects to form. Dry-jet wet spinning thus introduces an air gap that reduces the formation of such defects. In dry-jet wet spinning, an air gap is located between the exit of the spinneret and surface of the nonsolvent bath. The nascent filaments are extruded into air and drop into the bath. Thus, coagulation of the polymeric fiber begins prior to entry into the nonsolvent bath (Khayet, 2003). The external surface of the nascent fiber undergoes coalescence and orientation of polymer units in the air, enabling stress relaxation of the polymer chains (Khayet, 2003; Ahmad, 2019). For both forms of solution spinning, fibers may be collected by a roller or winding wheel. Like flat sheet membrane synthesis, the thermodynamics of solution spinning can be captured by the polymer/nonsolvent/solvent ternary phase diagram shown in Fig. 3.

The effects of spinning parameters on HF synthesis are well characterized for different applications. Such parameters are bore fluid type, bore fluid temperature, bore fluid flowrate, air gap distance, dope solution type, dope extrusion flowrate, dope extrusion pressure, dope viscosity, take-up speed, spinneret design, external nonsolvent type, external nonsolvent temperature, residence time, and coagulation bath depth (Ahmad, 2019). Modulation of these parameters can influence the structural integrity, morphology, and likelihood for defects of the resultant HFs.

The polymer dope solution type, and consequently its viscosity, is key to determining HF properties. Viscosity is a diffusional property of the dope solution, thus affecting phase inversion kinetics, in which nonsolvent-solvent mutual diffusion occurs and transfers the polymer from a liquid to solid state (Han, 2002; Giwa, 2017). The dope solution is primarily composed of two components, the polymer and solvent. A high concentration of polymer and therefore higher

viscosity of the solution reduces the membrane porosity and promotes chain entanglement of the nascent HF (Chang, 2008). HF spinning can only occur in a defined viscosity range, as too low of a viscosity may prevent sufficient coagulation of the polymer and too high of a viscosity may introduce problems such as the die swell effect, which distorts polymer flow as it exits the spinneret (Ahmad, 2019; Widjojo N. C., 2010). Solvent choice is dependent on the polymer, as they are typically selected based on the solubility of polymer within the solvent or miscibility with ethanol or water. As with flat sheet membranes, common solvents include NMP, DMSO, DMF, and DMAc (Ahmad, 2019).

The bore fluid type and external nonsolvent bath do not necessarily have to be the same compound, though they serve similar a similar function to coagulate the polymer dope solution. The bore fluid primarily dictates the internal surface morphology and initial solvent-nonsolvent exchange, while the external nonsolvent bath dictates the outer surface morphology and completes the phase inversion of the HF (Ahmad, 2019). Since bore fluid affects the initial rate of phase inversion, it allows for the establishment of the HF structure and prevents fiber collapse. A common strong bore fluid is water, with weaker bore fluids including DMSO, NMP, DMAc, and DMF. Faster coagulation leads to the formation of finger-like macrovoids, while slower coagulation leads to the formation of spongey structures. As for the external nonsolvent bath, a strong coagulant such as water will cause a dense and smooth outer surface to form, while a weaker coagulant such as an alcohol will lead to a porous outer surface. Flowing coagulants on two sides of HF membranes (interior and exterior) is one key distinction from the synthesis of flat sheet membranes. If the diffusion rate of nonsolvent at the HF exterior exceeds that of the diffusion rate at the interior, the outer layer can form large macrovoids and hold water, causing delamination of the interior and exterior layers. On the other hand, if the nonsolvent diffusion rate is lower at the

exterior compared to the interior, macrovoids and distortions form at the inner layer but adhesion is improved (Setiawan, 2012).

The residence time of the HF in air and air gap are closely linked. The residence time (RT) can be defined using the air gap (AG), take-up speed of the fiber by the drum (TS), and the speed at which the dope exits the spinneret (DS): $RT = \frac{2AG}{TS+DS}$ (Çulfaz, 2010). A high AG thus means that the RT is longer, leading to the formation of a thicker skin-layer on the surface of the HF (Ahmad, 2019). A high AG will also accentuate the effects of elongational and gravitational stress on the nascent HF as it is forming, especially at the outer surface. This creates a HF with a smaller diameter, tighter molecular packing, and molecular orientation, all of which reduce the final permeance and lead to finger-like macrovoids (Widjojo N. C., 2006). However, with a very high AG, the elongational stress may pull apart molecular chains as the nascent fiber is forming, causing high porosity in the HF. If the AG gap is too high, the elongational and gravitational stress may overwhelm the strength of the nascent HF, causing the fiber to break. Yet, the AG must also be high enough to ensure the interaction and adhesion of the inner and outer layers of the HF prior to immersion in the nonsolvent bath.

1.5 Thesis Overview

In this thesis, we will be investigating the synthesis and characterization of materials that can be used to purify and recycle spent dialysate for application in a portable dialysis device. We developed a set of design specifications that apply to both flat sheet and HF membranes. Chapter 2 will discuss the development of flat sheet polymer membranes for the separation of urea and glucose in dialysate. We investigate a broad range of parameters such as polymer type, casting temperature, and optional heat treatment and their effect on membrane performance, which was

measured via percent of urea and glucose permeated. Additionally, we investigate the kinetics of the flat sheet membrane synthesis process as well as general characteristics such as wettability. In doing so, we developed and optimized a flat sheet membrane capable of rejecting glucose while promoting urea flux in solution. The membrane was composed of a cellulose acetate matrix and the casting solution included mixed solvents and additives (acetone, dioxane, acetic acid, and methanol). The specific synthesis parameters included a 0℃ casting slide temperature, 0℃ nonsolvent bath temperature, and 1 h of thermal treatment at ~65℃.

Chapter 3 focuses on the translation of flat sheet membranes to HF membranes. Harnessing the kinetics experiments conducted for flat sheet membranes, we performed a systematic review of air gap, dope extrusion flowrate, and bore fluid extrusion flowrate. We critically assessed problems such as die swelling, solvent-nonsolvent exchange rate, elongational/gravitational stress, and formation of imperfections until we were able to reliably generate HFs with the characteristic hollow cylindrical morphology. We elected to control for the spinneret dimensions, bore fluid composition, and nonsolvent bath composition throughout all experimentation. We additionally investigated the effect of polymer type on HF morphology. We found that PES HFs showed the most promise for filtration, given their robust structure, minimal delamination, slightly improved wettability (relative to PSF), and improved demixing rates.

Chapter 2: Synthesis and Optimization of a Flat Sheet Membrane

2.1 Introduction

Flat sheet membranes are widely applied for filtration and purification applications. They are easy to synthesize in bulk and have many synthesis parameters that can be modulated to tune their properties. We aim to synthesize and optimize a flat sheet membrane such that 240 mmol (14 g) of urea can be separated from glucose in dialysate in 7-9 h. This rate of clearance mimics that of a healthy kidney and poses a good baseline goal. We require that this filtration be functional for spent dialysate with a high glucose concentration, as dialysate can hold 70 – 130 mg/dL of glucose (Baura, Medical device technologies: A systems based overview using engineering standards (Second ed.), 2021). We envision that the filtered urea can then be electrodecomposed into N2 and CO2 through a previously developed TiO2 nanowires system without the risk of oxidation of glucose into toxic byproducts such as gluconic acid and glucaric acid (Shao, 2019; Yin, 2020). Urea has a molecular weight of 60 Da, while glucose is three times larger at 180 Da. The size of a single urea molecule has been estimated to be 0.3x0.497x0.534 Angstrom (Stein, 1986). The size of a single glucose molecule has been estimated to be 1.5 nm (Minoli, 2005). We thus expect a functional membrane to have pore sizes ranging from 0.1-1 nm with high monodispersity.

In this chapter, we also aim to perform material characterization of flat sheet membranes to critically assess their suitability for hollow fiber membranes. Of particular importance is the rate of solvent-nonsolvent exchange that is strongly correlated with solution viscosity, as hollow fiber spinning cannot take place outside of a defined range of viscosities. These results inform our approach to synthesizing a hollow fiber membrane using parameters resembling that of our flat sheet membranes.

2.2 Materials and Methods

2.2.1 Experimental Design

We evaluated the composition and procedural parameters listed in Table 2. Compositional parameters were optimized first to establish a cast solution with desirable flux properties. Due to time and cost constraints, we did not employ a full factorial design for all the procedural parameters. We utilized a full factorial design (2^2) for the slide temperature and bath temperature parameters. For the remainder of the procedural parameters, we progressed in a sequential manner, in which we optimized for one parameter at a time, then moved to the next. Table 3 displays several factors and levels in a mixed-level design.

Type	**Parameters**
Compositional	Polymer type, polymer concentration, organic additives
Procedural	Slide temperature, nonsolvent bath temperature, $+/-$ thermal annealing, annealing temperature

Table 1. Membrane parameters evaluated, organized into compositional and procedural categories.

Factor	**Unit**	**Levels**		
		-1	**0**	**+1**
Casting thickness	µm	100	200	400
Slide temperature	℃	N/A	0	25
Bath temperature	℃	N/A	0	25
Heat treatment temperature	℃	65	70	80

Table 2. Design of experiments table of factors and mixed levels.

2.2.2 Reagents and Materials

Polymers tested included polysulfone (avg. Mn ~3000, Sigma Aldrich), polyethersulfone (avg. Mn ~22000, Sigma Aldrich), polyimide (TECAPOWDER P84 solution grade, Ensinger), polyetherimide (Sigma Aldrich), and cellulose acetate (avg. Mn ~30000, Sigma Aldrich). Solvents and organic additives included N-methyl-2-pyrrolidone (anhydrous, 99.5% purity, Sigma Aldrich), 1,4-dioxane (anhydrous, 99.8% purity, Sigma Aldrich), acetone (HPLC grade, 99% purity, Fisher Chemical), acetic acid (glacial, >99% purity, Sigma Aldrich), and methanol (HPLC grade, >99.9% purity, Sigma Aldrich).

2.2.3 Membrane Synthesis

We used the well-characterized phase inversion immersion precipitation method to synthesize the membranes, as demonstrated in Fig. 5. Briefly, a casting solution was created by combining polymer, organic solvent, and additives when applicable. The solution was placed on a horizontal shaker at 120 rpm for three days or until homogenous. The solution was cast onto a glass slide support (room temperature or ice cold) with a doctor blade (MTI Corporation KTQ-80F) at a thickness of 200 µm. After a set evaporation time, the glass slide with cast solution was immersed in a MilliQ water bath for a minimum of 6 h. Following synthesis, membranes underwent an optional heat treatment/thermal annealing step, in which they were immersed in a 60-80℃ water bath for 1 h. Membranes were cut and stored in DI water (MilliQ, 18.2 MΩ) at room temperature.

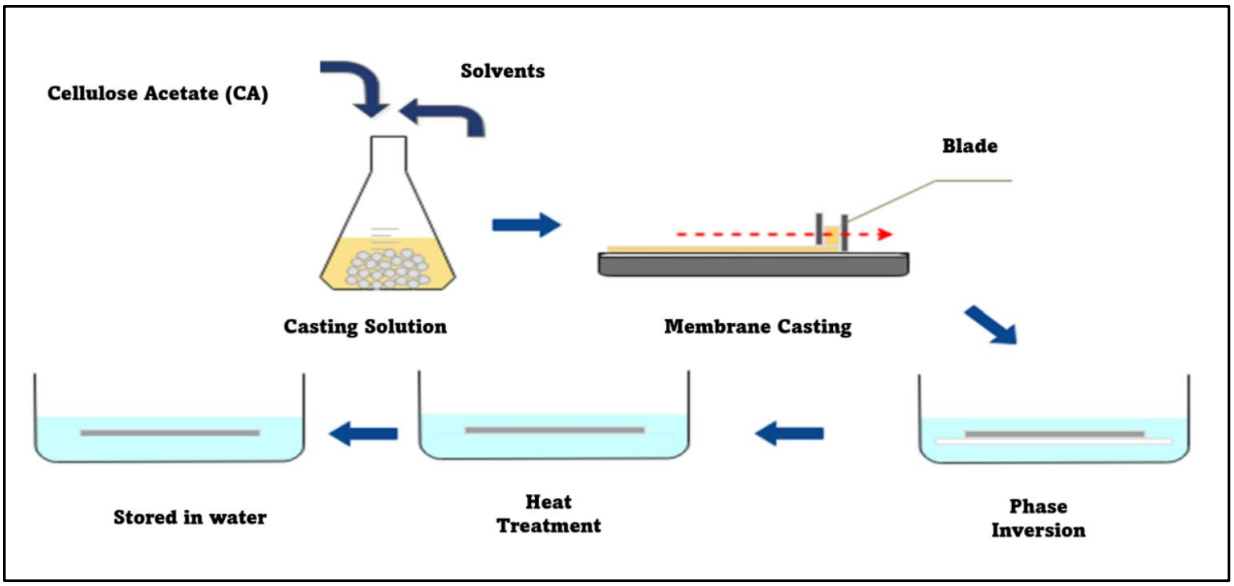

Fig. 5. Membrane synthesis schematic using a cellulose acetate base (Kassim Shaari, 2017).

2.2.4 Permeability Measurements

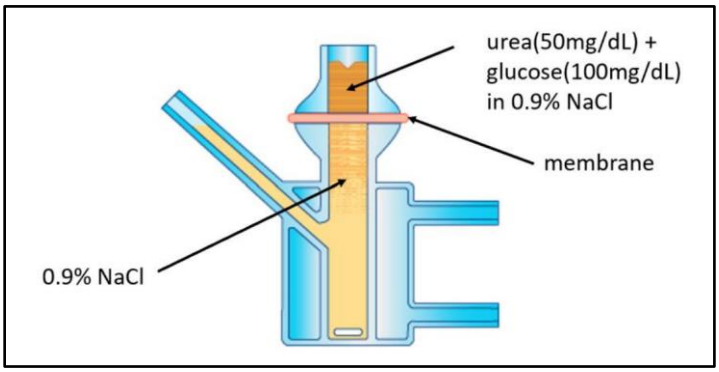

Figure 6. Schematic of permeability measurement using a Franz diffusion cell.

A Franz diffusion cell (PermeGear, #4G-02-00-25-20) was used to measure permeability of membranes (Fig. 6). In a standard measurement, the bottom chamber was loaded with 20 mL of 0.9 wt% NaCl and the top chamber was loaded with 10 mL of a 50 mg/dL urea and 100 mg/dL glucose in 0.9 wt% NaCl solution. The membrane was sandwiched between the top and bottom chambers. A magnetic stir bar was placed inside the lower chamber. After 45 min of magnetic stirring (until equilibrium), 6 mL of supernatant was collected from the top and bottom chambers. We measured the concentration of urea and glucose in each sample of supernatant using a clinical chemical analyzer (AU680, Beckman Coulter). The selectivity ratio was calculated using the following formula: $R = \frac{\%\ urea\ permeated}{\%\ glucose\ permeated} \times 100\%$.

2.2.5 Permeability Measurements

To evaluate the mass transport properties of the membranes, we collected supernatant samples from the top and bottom chambers at several time points: 5 min, 10 min, 20 min, and 45 min. The glucose and urea concentration for the collected samples were measured using a clinical chemical analyzer (AU680, Beckman Coulter). The permeated mass for glucose and urea were calculated as so: $Mass = C_{bottom} \times V_{bottom} \times MW$, where C_{bottom} is the concentration in the bottom chamber and $V_{bottom} = 20\ mL$ is the volume of the bottom chamber.

2.2.6 Material Characterization

To assess the wettability of the synthesized materials, we performed contact angle measurements. A 1 cm x 1 cm piece of the membrane was cut, placed on the stand, fixed with tape, and dried of any water on the surface. A drop of water was deposited on the membrane using a micropipette and the contact angle was collected.

To evaluate the solvent-nonsolvent exchange (demixing) rate, we measured the detachment time and time to opacity. The detachment rate was defined as the time from initial immersion into the nonsolvent bath until the precipitated polymer membrane began to detach from the glass support. The time to opacity was defined as the time at which the opacity of the membrane reached its maximum. A video camera was mounted and captured the phase inversion process of the membrane, and the videos were analyzed afterwards for the time to opacity.

2.2.7 Scanning Electron Microscopy

Scanning electron microscope (SEM) images were obtained using a SNE-3200M scanning electron microscope (NanoImages, LLC). Membranes were dried thoroughly and sputter coated with gold prior to imaging. Accelerating voltage was set to 5 or 10 kV, the detection mode was set to scanning electron mode, and the magnification ranged from 500X to 3000X.

2.3 Results and Discussion

2.3.1 Effect of Casting Thickness

To determine the ideal casting thickness, we cast PSF flat sheet membranes at thicknesses of 100 µm, 200 µm, and 400 µm onto the glass support prior to immersion in the nonsolvent bath. The resulting SEM images are shown in Fig. 7. The 100 µm casting thickness led to a 6-8 µm membrane with 1-2 µm pore sizes. The 200 µm casting thickness led to a 14 µm membrane with a distinct dense skin layer and finger-like macrovoids. The 400 µm casting thickness led to a >20 µm membrane with a dense surface layer, smaller pores, and macrovoids of varied sizes. The pore size distribution resulting from the 100 µm casting thickness is unfortunately not within the desired range for separation, as glucose is estimated to be 1.5 nm in size. The thickness of the membrane cast at 400 µm is likely to inhibit efficient flux, and the morphology is less consistent than that of the membrane cast at 200 µm. The polymer-dense skin layer of the 200 µm cast membrane provides selectivity between urea and glucose; the polymer-lean macrovoids allow for efficient mass transport and provide mechanical support for the skin layer. Therefore, we selected the 200 µm casting thickness for subsequent experimentation.

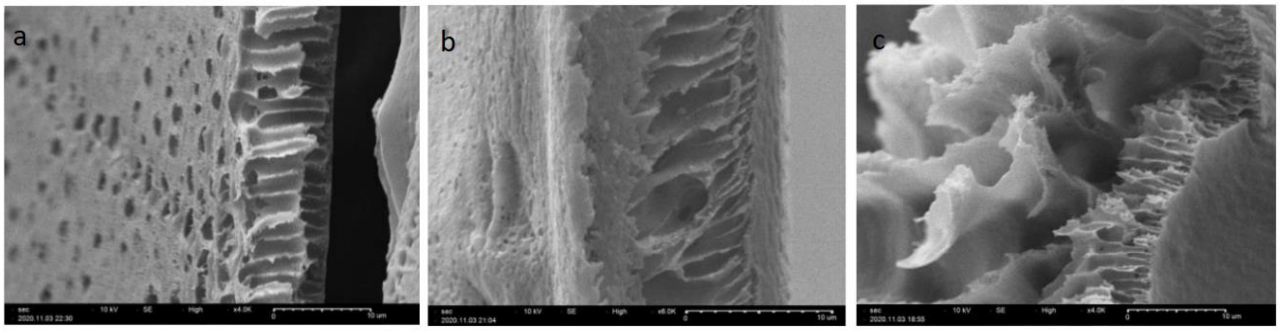

Fig. 7. SEM images depicting PSF membrane morphology for casting solution thickness of a) 100 µm, b) 200 µm, and c) 400 µm.

2.3.2 Effect of Polymer Type and Concentration

Given the many polymer types available commercially and used for industrial applications, we evaluated the effect of polymer type and concentration on separation performance for urea and glucose. Fig. 8 shows the range of concentrations for each of four selected polymers (PSF, PES, P84, and CA) dissolved in NMP. Both PSF and PES show a clear cutoff concentration at which no urea or glucose is able to permeate. However, 16 wt% PSF membranes show no permeance of urea or glucose, while 16 wt% PES membranes have substantial permeation. The larger size of one PES unit compared to PSF unit may contribute to the observed higher pore size at the same concentration. Furthermore, PES is more hydrophilic than PSF due to the presence of multiple sulfone functional groups. The improved hydrophilicity of PES promotes the rate of demixing between NMP and water, resulting in a pore distribution with a higher average. At higher concentrations of PSF (≥16 wt%) and PES (≥18 wt%), the higher concentration of polymer at the polymer/nonsolvent interface at the instant of immersion generates a thicker skin layer, therefore slowing the demixing of solvent and nonsolvent. A spongier structure with smaller pore sizes is therefore generated.

P84 and CA show high permeance of urea and glucose across all concentrations, with urea permeance peaking at >14% and glucose permeance peaking at >9%. The urea permeance does not drop <10% and the glucose permeance does not drop <3% even at the highest concentrations. The reduced glucose permeance in this case is caused purely by its increased molecular weight; the rate of diffusion is inversely proportional to molecular mass. These results are indicative of a thin, porous skin layer. However, we were unable to pursue higher concentrations of P84 and CA as the polymer becomes very challenging to dissolve in NMP without introducing additional factors such as heat.

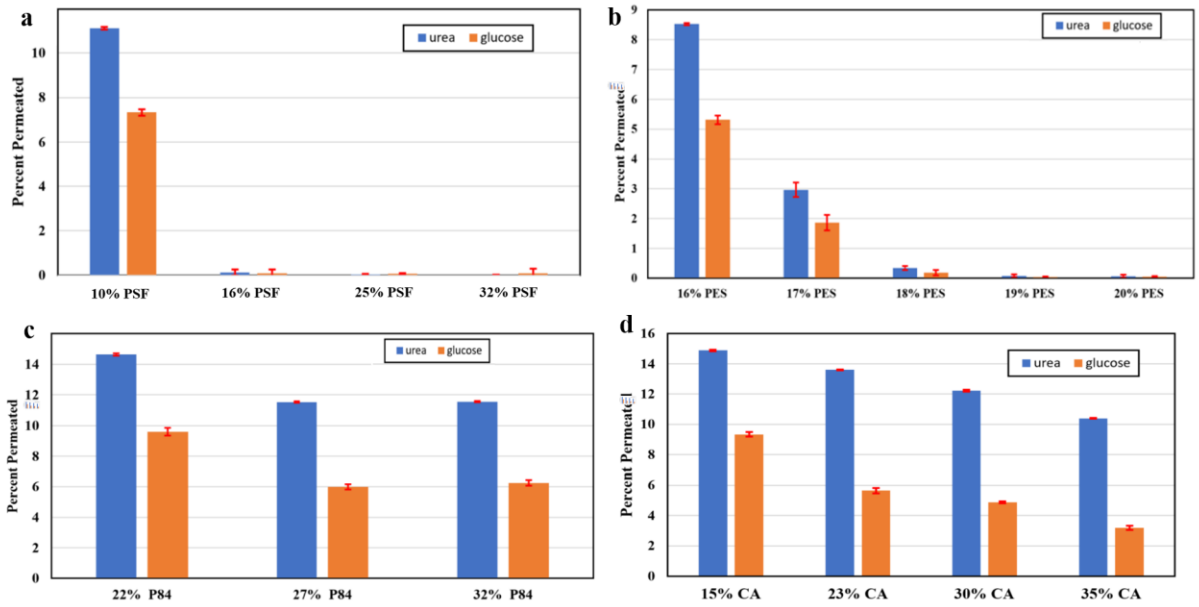

Fig. 8. Percent of urea and glucose permeated for a) 10-32 wt% PSF, b) 16-20 wt% PES, c) 22-32 wt% P84, and d) 15-35 wt% CA dope solutions with NMP as solvent.

2.3.3 Effect of Thermal Annealing

We investigated the effect of thermal annealing (heat treatment) after membrane synthesis for several different polymers. From Fig. 9a, thermal annealing was found to have little effect on improving the permeation ratio for PSF. However, Fig. 8b shows that annealing for 1 h at 80ºC dramatically improved the urea/glucose permeation ratio for CA, particularly for the 23, 30, and 40 wt% dope solutions. Thermal annealing densifies the structure of the polymer matrix by shrinking voids between aggregates and intramolecular segments, causing more efficient chain packing. While chain packing had minimal effect on PSF, it was able to shrink the pore distribution of 23-40 wt% CA membranes such that glucose was rejected but urea was still able to permeate. We observe that at 45 wt% CA, the performance of the membrane experiences a significant drop off with the heat treatment condition. This indicates that between 40 and 45 wt%, CA membranes are too dense to permit permeation of urea or glucose and thus do not have an observable response to thermal annealing.

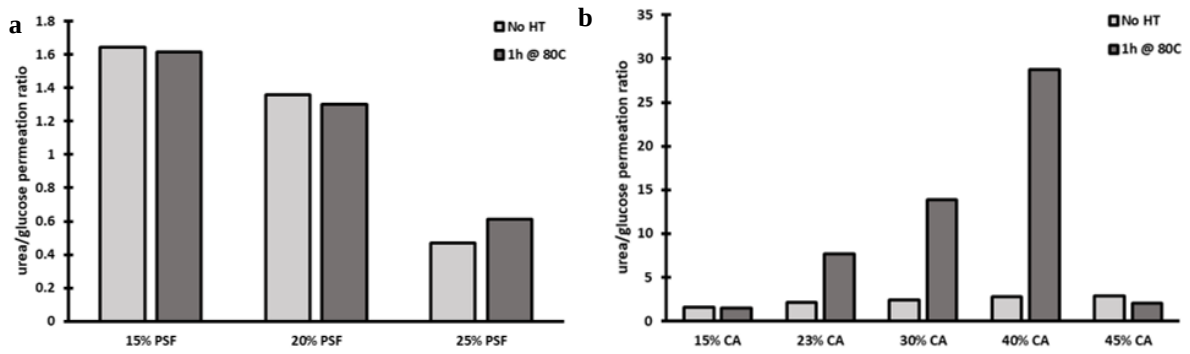

Fig. 9. Urea to glucose permeation ratio for a) 15-25 wt% PSF and b) 15-45 wt% CA with a no treatment condition and a 1 h heat treatment at 80ºC condition.

2.3.4 Effect of Organic Additives

Given the promising effect of thermal annealing for CA membranes, we next sought to improve the solvent composition of CA dope solutions with additives. The mixed solvent composition of 45.77 wt% dioxane, 17.61 wt% acetone, 8.45 wt% acetic acid, and 14.09 wt% methanol was drawn from literature (Duarte, 2006). CA has excellent solubility in dioxane and acetone. Acetone has also been shown to slow the precipitation of polymer after immersion. Acetic acid is a softener that improves polymer chain mobility. Finally, methanol is a nonsolvent that promotes miscibility of water into the polymer/solvent system after immersion.

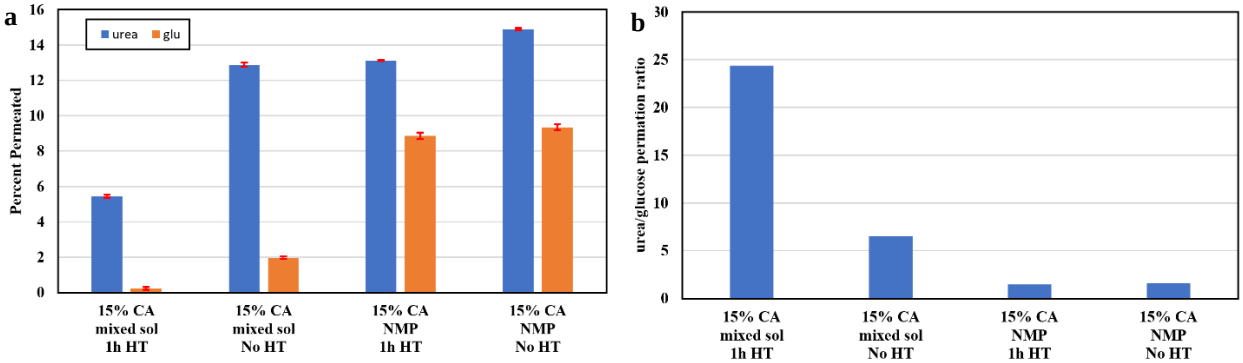

Fig 10. a) Urea and glucose permeation for 15 wt% dope solutions with varied solvents and +/- thermal annealing. b) Urea to glucose permeation ratio for the conditions in (a). Mixed sol: 45.77 wt% dioxane, 17.61 wt% acetone, 8.45 wt% acetic acid, and 14.09 wt% methanol. HT: heat treatment for 1 h at 80ºC in water.

Fig. 10 illustrates that the mixed solvent condition yielded improved urea to glucose permeation, even without thermal annealing. Annealing the samples with NMP as the solvent had

little effect on improving the urea to glucose permeation ratio, although the overall flux for both molecules decreased as shown in Fig. 10a. Between the annealed and unannealed mixed solvent samples, the annealed sample yielded a 3.5X improvement in permeation ratio. The enhanced response of the mixed solvent samples to thermal annealing is potentially caused by the incorporation of acetone as a polymer softener, enabling greater chain mobility when exposed to heat. Despite the promising urea to glucose permeation ratio, Fig. 10a shows that the overall flux of urea in the annealed mixed solvent condition is quite low at <6%.

2.3.5 Effect of Synthesis Temperature

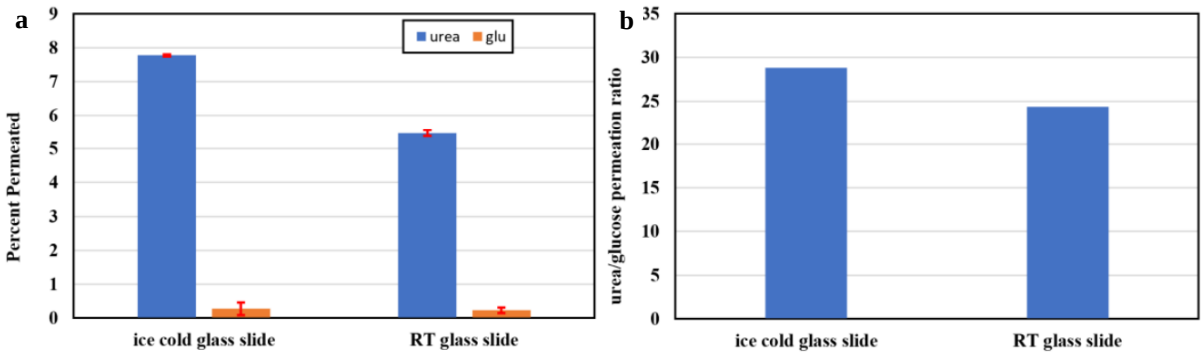

Fig. 11. a) Urea and glucose permeation for 15 wt% CA in mixed solvent with an ice cold glass slide condition and room temperature (RT) glass slide condition. b) Urea to glucose permeation ratio for the conditions in (a).

Synthesis temperature is a determining factor of the solvent-nonsolvent exchange rate. At lower temperatures, demixing is delayed; at higher temperatures, demixing may be instantaneous. Though this effect of nonsolvent bath temperature is understood, the effect of the glass support temperature is less well characterized. Thus, we cast membranes with a dope solution of 15 wt% CA in mixed solvent on an ice cold glass slide and a room temperature glass slide, then immersed the slide in an ice cold nonsolvent bath (Fig. 11). In both conditions, glucose permeation was near zero. Thus, casting the solution on an ice cold slide specifically improved urea permeation by over 2%. We speculate that the decreased temperature slowed the evaporation of solvent prior to immersion, thus slowing the formation of a denser layer of polymer at the top of the cast solution

and resulting in a more porous skin layer. Immersing the slide in the 0ºC nonsolvent bath then slows the solvent/nonsolvent exchange, allowing for the formation of a spongier, more uniform membrane with a narrower pore distribution.

2.3.6 Combined Effect of Synthesis Temperature and Thermal Annealing

We then examined the effect of ice cold synthesis temperatures in combination with thermal annealing. From Fig. 12c, a room temperature slide with no annealing has poor separation performance. Annealing eliminates glucose flux by mobilizing the polymer chains and shrinking pores but reduces the urea permeation by 2.4X compared to the no annealing condition. Synthesizing the membrane with an ice cold slide and annealing improves the urea flux compared to the only annealing condition by 1.4X while maintaining zero glucose permeation. We estimate using extrapolation that the time for 14 g of urea filtration given a 1 m^2 membrane is roughly 10 h. We would like to minimize this time to under 8 h.

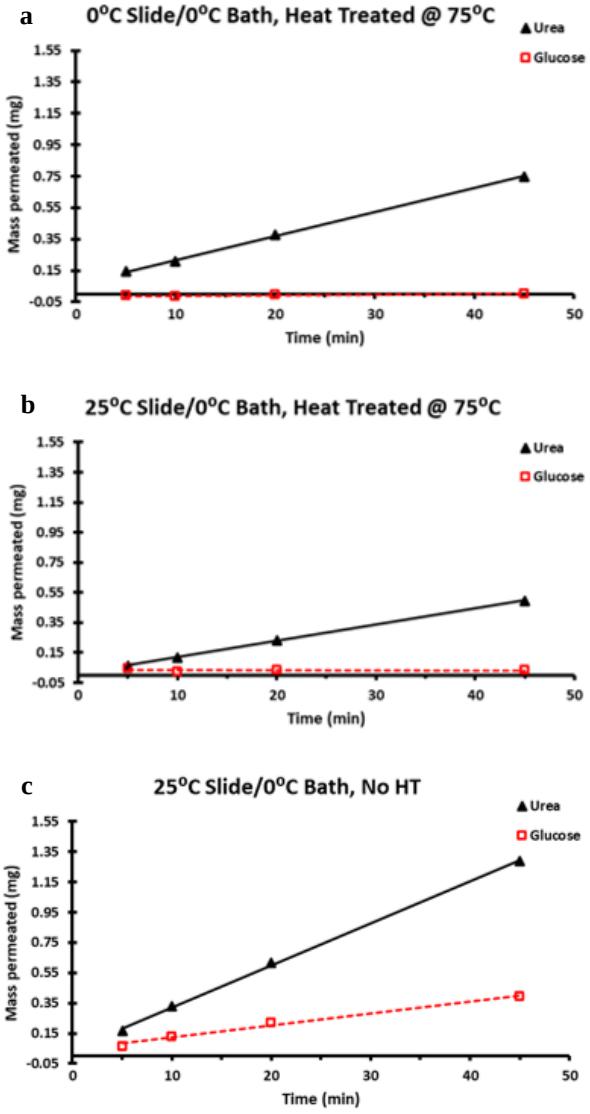

Fig. 12. Mass permeated for urea and glucose at 5, 10, 20, and 45 min time points for a) ice cold glass slide & annealing, b) room temperature (25ºC) glass slide & annealing and c) room temperature (25ºC) glass slide & no annealing. All membranes were synthesized with mixed solvent CA solution and ice cold nonsolvent bath conditions.

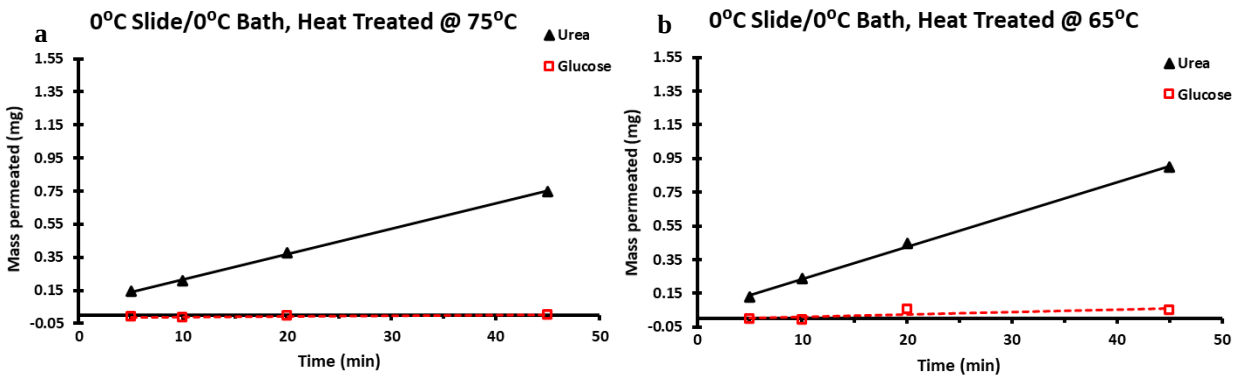

Fig. 13. Mass permeated for urea and glucose at 5, 10, 20, and 45 min time points for membranes synthesized with a 1 h annealing temperature of a) 75ºC and b) 65ºC. All membranes were synthesized with mixed solvent CA solution and ice cold slide and bath conditions.

Since thermal annealing causes chain packing, we investigated the effect of different annealing temperatures (65ºC, 70ºC, 75ºC, and 80ºC) while keeping the total time fixed at 1 h (Fig. 14). We found that between 65 ºC and 80ºC, the urea permeation is linearly correlated to the temperature. Thus, we can infer that the degree of chain packing is also linearly correlated to the temperature. Of note, the data point for the no annealing temperature follows this linear relationship and falls around the point for 60ºC. Thus, we concluded that annealing at temperatures under 65ºC have a negligible effect on the polymer structure, as insufficient energy is transferred to the chains for mobilization. At exactly 65ºC, we were able to improve the urea permeation through the membrane without compromising the zero glucose flux (Fig. 13). With the 65ºC annealing condition, our membrane is estimated to permeate 14 g in 6 h (Fig. 14).

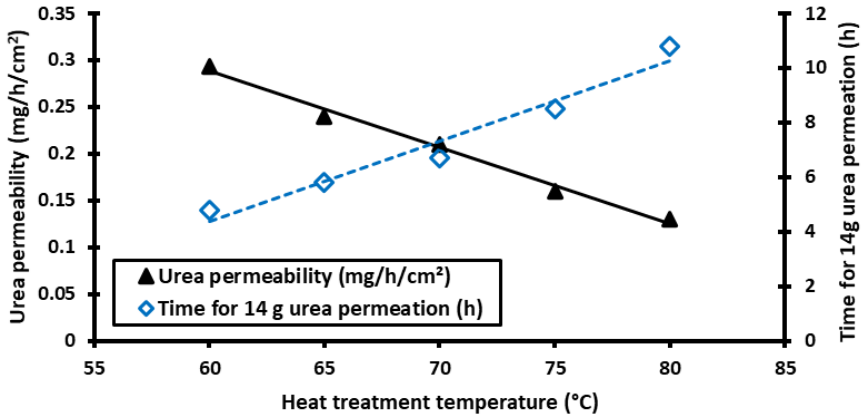

Figure 14. Urea permeability and time for 14 g urea permeation vs. thermal annealing temperature.

2.3.7 Membrane Wettability

Having successfully synthesized and optimized a flat sheet membrane for separation of urea and glucose, we sought to further characterize the materials to facilitate the conversion to hollow fibers. This characterization is additionally important as a preliminary assessment of our synthesized materials in a system with real dialysate, which may have proteins such as albumin circulating in addition to uremic toxins, glucose, and electrolytes. Since proteins usually have hydrophilic residues with water molecules and counterions bound on their exterior, contact with membrane surfaces causes proteins to liberate the bound water molecules and counterions (Ji, 2023). This induces conformational changes that expose hydrophobic residues, resulting in adsorption to the hydrophobic membrane surface. Thus, materials used in a portable dialysis system should ideally have improved hydrophilicity.

We measured the contact angles of several different polymeric membranes across different concentrations of dope solutions. The specific concentrations were selected based on membranes synthesized in previous experiments. We found that the 16 wt% PSF sample was the most hydrophobic of all the membranes with an average contact angle of 81.17º (Fig. 15). Increasing the concentration of PSF to 25 wt% measurably improved the wettability of the membrane but increasing the concentration further to 32 wt% did not further change the wettability.

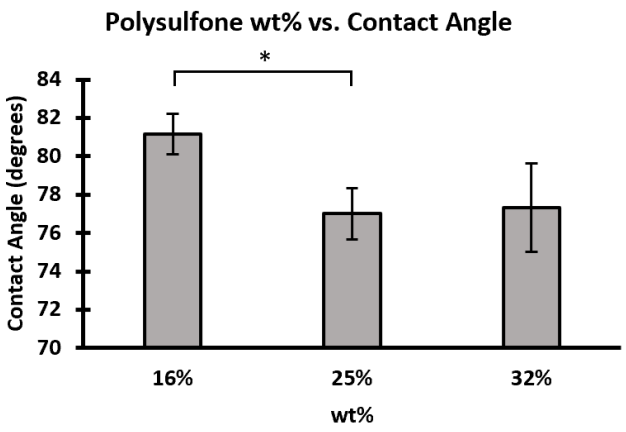

Fig. 15. Contact angle of membranes synthesized with dope solutions of 16, 25, and 32 wt% PSF in NMP.

We performed similar measurements for 16, 18, and 20 wt% PES (Fig. 16). Again, we found that the lowest concentration of 16 wt% PES was the most hydrophobic at 78.17º. The slightly lower contact angle compared to PSF solutions of the same concentration are likely attributed to the increased concentration of sulfone groups in one PES unit that promote water affinity. We again observe that increasing the concentration of PES in solution results in somewhat of a decrease in contact angle, but that there is no significant difference between the 18 wt% and 20 wt% conditions.

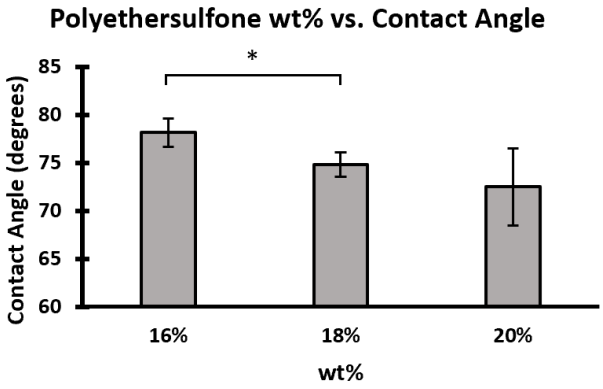

Fig. 16. Contact angle of membranes synthesized with dope solutions of 16, 18, and 20 wt% PES in NMP.

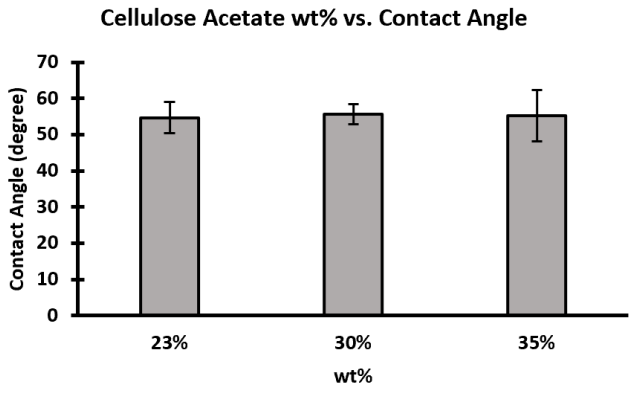

Fig. 17. Contact angle of membranes synthesized with dope solutions of 23, 30, and 35 wt% CA in NMP.

Finally, we performed contact angle measurements for 23, 30, and 35 wt% CA in NMP (Fig. 17). We elected not to use the mixed solvent solution so as to not introduce an additional confounding variable in our analysis of the polymer itself. Of the three polymers, CA membranes demonstrated the highest degree of wettability at contact angles of 50-60º. There was no significant difference between the membranes prepared with dope solutions of different concentrations. Fig. 18 summarizes the contact angle findings for all dope solutions tested.

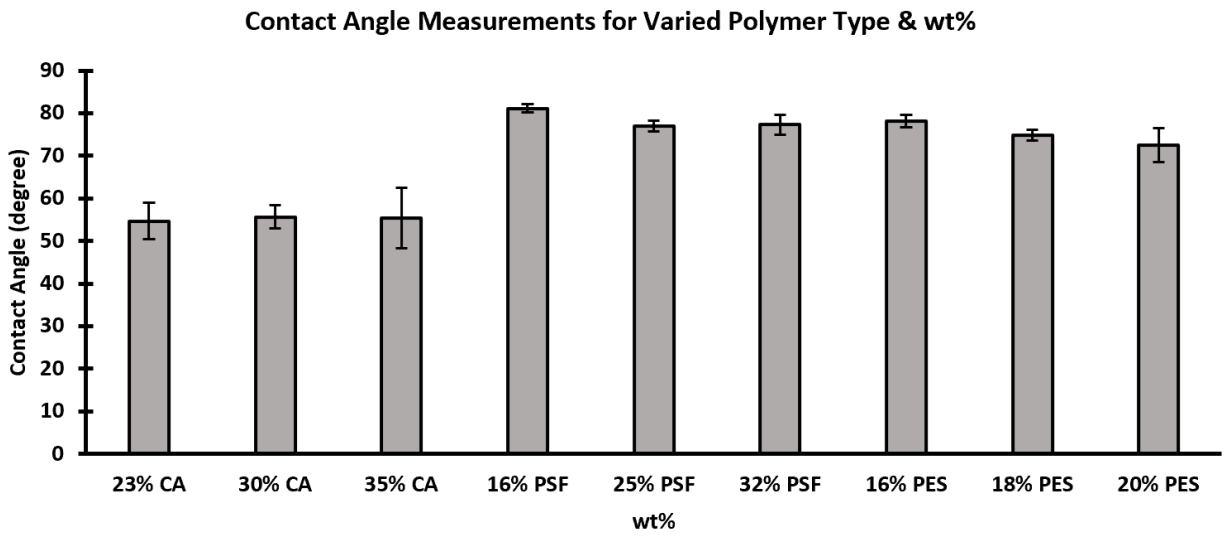

Fig. 18. Contact angle of CA, PSF, and PES membranes with NMP as nonsolvent.

Interestingly, the results for PSF and PES are not consistent with our expectations. We expect that low polymer concentration leads to more rapid demixing of solvent and nonsolvent, which promotes the formation of macrovoids and larger pores through which water flux can occur. Conversely, high polymer concentration would cause the formation of a denser skin layer that slows demixing, resulting in a spongier and denser membrane. Therefore, we expect that lower polymer concentrations would have improved wettability, while higher concentrations would exhibit lower wettability. One potential explanation for our results is that all membranes were dried prior to measurement. Given the channeled and more porous morphology of the membranes from low wt% solutions, water that permeated through the membrane was perhaps easier to evaporate than water trapped within the denser matrix of membranes from high wt% solutions. If some residual water was present in the denser membranes, they may have been measured to have a lower contact angle.

2.3.8 Solvent-Nonsolvent Exchange Rate

We next sought to examine the solvent-nonsolvent exchange rate, as it is arguably the most important factor in determining whether hollow fibers can be successfully synthesized. We elected

to measure the exchange rate in two ways. The first was measuring the amount of time between immersion of the casted solution and detachment of the precipitated membrane from the glass support, termed "detachment time". The second was measuring the amount of time between immersion of the casted solution and full opacity of the precipitated membrane, termed "time to opacity" (though not all membranes became fully opaque).

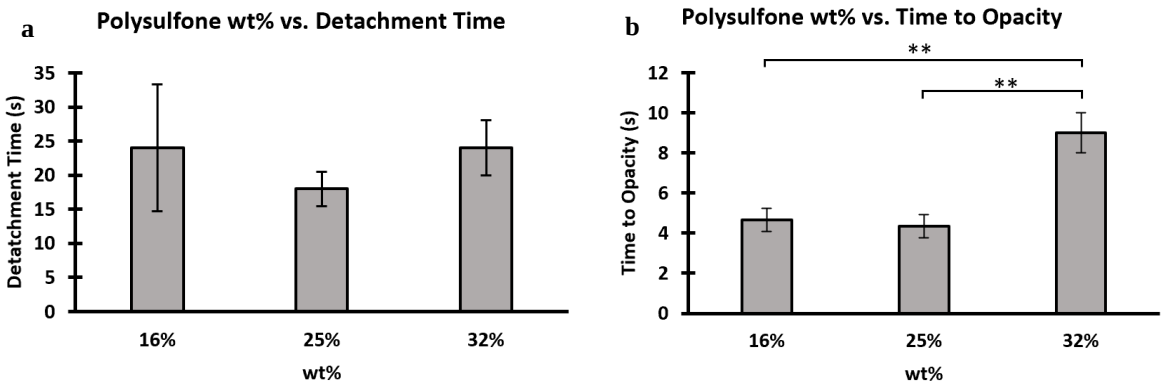

Fig. 19. a) Detachment times and b) times to opacity for membranes synthesized from 16, 25, and 32 wt% PSF in NMP solutions.

PSF membranes with 16, 25, and 32 wt% solutions did not exhibit a statistically significant difference in detachment time (Fig. 19). All membranes detached from the slide at an average time of 18 to 24 s. Perfect detachment time measurements depend on a uniform and consistent solution cast onto the glass support. The front and back ends of the cast solution tend to have much higher thickness than the uniform middle section due to the nature of casting; the blade pushes the solution down the slide, and residual solution is deposited at the end of the membrane. Thus, lifting of the membrane may have been affected by the thicker deposits of polymer on both ends. However, for the opacity measurements, which are unaffected by the deposits of polymer, it was found that there was a substantial increase in the time to opacity for the 32 wt% membranes. 16 wt% and 25 wt% membranes had an average time to opacity of 4.67 s and 4.33 s respectively. 32 wt% membranes had an average time to opacity of 9 s, indicating that there is slower solvent-nonsolvent exchange with the increased concentration of PSF.

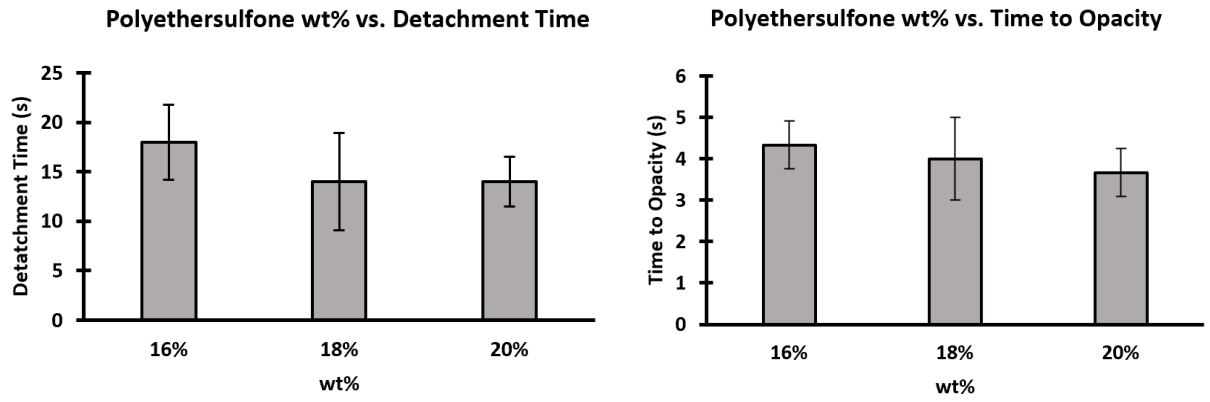

Fig. 20. a) Detachment times and b) times to opacity for membranes synthesized from 16, 18, and 20 wt% PES in NMP solutions.

16, 18, and 20 wt% PES membranes similarly did not have a significant difference in detachment times or times to opacity, which may be partially attributed to the polymer deposition situation outlined in the previous paragraph (Fig. 20). However, it is likely that the range of PES concentrations was too narrow to notice any appreciable differences at the synthesis step, even if detectable after measuring permeability.

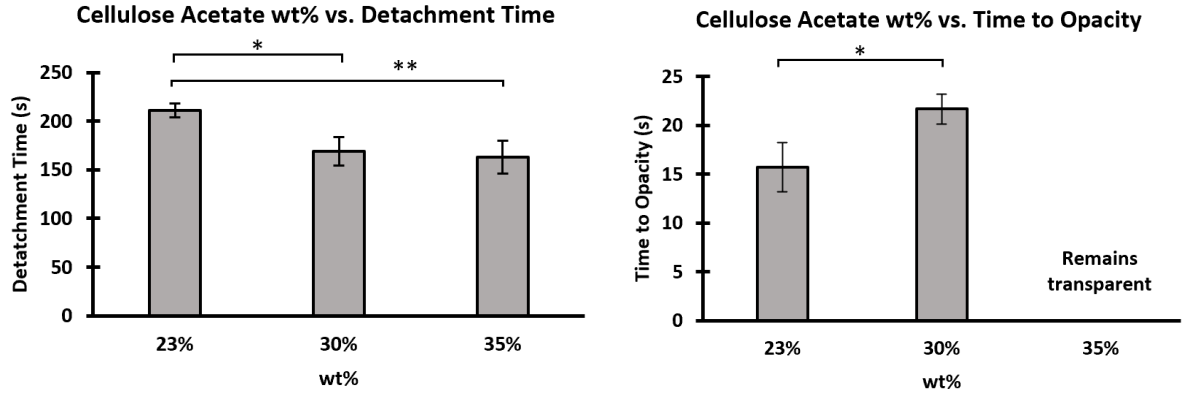

Fig. 21. a) Detachment times and b) times to opacity for membranes synthesized from 23, 30, and 35 wt% CA in NMP solutions.

CA membranes exhibited decreasing detachment time as polymer concentration increased. The 23 wt% membranes had the longest average detachment time of 211 s, followed by 169 s for the 30 wt% membranes and 163 s for the 35 wt% membranes. These results are initially counterintuitive, as detachment time is a theoretical measure of when enough demixing has

occurred for the membrane to detach from the slide. However, higher concentrations of polymer cause denser and thicker skin layers that may be more prone to detaching from the slide, even if demixing has not fully resolved within the center of the membrane. This is because the 35 wt% solution is thermodynamically less stable with less nonsolvent needed for precipitation. Simultaneously, it demonstrates slowed kinetics, with the time to opacity results confirm that demixing is indeed occurring more slowly as concentration of CA increases. In fact, the 35 wt% membrane never reaches opacity and remains translucent, even after remaining in the nonsolvent bath for over 15 minutes.

2.4 Conclusions

We synthesized and analyzed the effects of a wide range of parameters on the performance and morphology of polymeric membranes. After evaluating polymer type, casting thickness, thermal annealing, organic additives, and synthesis temperature, we found the following parameters outlined in Table 3 to be optimal. We achieved a >30 urea to glucose permeability ratio with excellent flux enabling 14 g of urea permeation in 6 h. In the following chapter, we will evaluate the conversion of our optimized flat sheet membrane into hollow fibers. The geometry of flat sheet membranes requires a support for incorporation into filtration systems, which is unwieldy and more challenging to manage compared to hollow fiber cartridges. Furthermore, if flat sheet membranes are to be used, the production needs to be scaled up from benchtop without introducing imperfections such as holes and bubbles in the material. For example, annealed membranes tend to be soft and more easily damaged immediately after removal from the heated bath. For these reasons, we hope to convert our synthesis technique from flat sheet membranes to hollow fiber membranes while maintaining the same high performance.

Parameter	Condition
Dope solution composition	14.09 wt% cellulose acetate, 45.77 wt% dioxane, 17.61 wt% acetone, 8.45 wt% acetic acid, and 14.09 wt% methanol
Nonsolvent bath composition	Water
Casting thickness	200 µm
Slide temperature	0ºC
Bath temperature	0ºC
Thermal Annealing +/-	+
Annealing bath composition	Water
Annealing temperature	65ºC

Table 3. Optimized parameters for separation of urea and glucose in dialysate.

Chapter 3: Conversion to Hollow Fiber Membranes

3.1 Introduction

Hollow fiber membranes have superior surface area to volume ratio than flat sheet membranes and are therefore widely employed in filtration applications from microfiltration to reverse osmosis. Like flat sheet membranes, the separation properties of hollow fibers are achieved by the dense skin layer. Larger macrovoids facilitate transport and provide structural support for the membrane. Due to the low packing density (membrane area to packing volume) of flat sheet membranes, they require more support in order to be incorporated into systems. Hollow fibers can be easily compacted into cartridges and sealed using epoxy resin for a space-efficient filtration unit.

We aim to develop a hollow fiber membrane with performance properties comparable to that of the flat sheet membranes. However, although hollow fiber membranes theoretically utilize the same phase inversion techniques, the formation mechanism is far more complicated than that for flat sheet membranes (Peng, 2012). One of the most important considerations for hollow fiber synthesis is the polymer dope solution formulation and properties. The polymer dope must stay within a specific viscosity range that is much higher than what is necessary for flat sheet membranes. This is because viscosity is a strong determinant of phase inversion kinetics. A high viscosity leads to slower demixing and a sponge-like structure in the synthesized membrane. If the viscosity is too high, the solution demixes too slowly and does not become structurally stable enough to form a hollow fiber. A high viscosity solution is also susceptible to high sheer stresses. On the other hand, too low of a viscosity may not be able to withstand the gravitational forces exerted on the nascent fiber during spinning, and the fiber may break before full demixing.

In this chapter, we investigate the replication of flat sheet membrane synthesis conditions for hollow fiber membranes. We perform a preliminary mathematical analysis of the additional shear and elongational stresses imposed on hollow fibers that are not present in flat sheet membrane production, and its potential effect on hollow fiber morphology and performance. We investigate the morphology of hollow fibers spun from different polymer dope compositions, harnessing the material characterization results from the previous chapter to analyze the kinetics of membrane formation in each case. Following this analysis, we present future directions and parameters of interest for how to further optimize HFs for separation of urea and glucose.

3.2 Materials and Methods

3.2.1 Reagents and Materials

Polymers tested included polysulfone (avg. Mn ~3000, Sigma Aldrich), polyethersulfone (avg. Mn ~22000, Sigma Aldrich), polyetherimide (Sigma Aldrich), and cellulose acetate (avg. Mn ~30000, Sigma Aldrich). Solvents included N-methyl-2-pyrrolidone (anhydrous, 99.5% purity, Sigma Aldrich), 1,4-dioxane (anhydrous, 99.8% purity, Sigma Aldrich), acetone (HPLC grade, 99% purity, Fisher Chemical), and acetic acid (glacial, >99% purity, Sigma Aldrich), methanol (HPLC grade, >99.9% purity, Sigma Aldrich). Spinning equipment included a spinneret with a 18G outer needle and 23G inner needle (SKE, EFA035) and syringe pump (Thermo Fisher Scientific, M361 Multi-Rate Infusion Pump).

3.2.2 Mathematical Analysis

Mathematical analysis of hollow fiber spinning was accomplished using MATLAB software.

3.2.3 Hollow Fiber Synthesis

Given the exact parameters of the flat sheet membrane synthesis, we sought to replicate the conditions for hollow fiber synthesis. Therefore, we acquired a spinneret with a 18G outer needle (OD = 1240 µm, ID = 840 µm) and 23G inner needle (OD = 635 µm, ID = 330 µm) (Fig. 22). With these needle dimensions, the extruded dope solution has a thickness of 205 µm, mimicking the 200 µm casting thickness of the flat sheet membranes. We selected a spinneret length (dimension F in Fig. 22) of 5 mm such that the length to annular thickness ratio exceeds 10, enabling approximation of laminar flow.

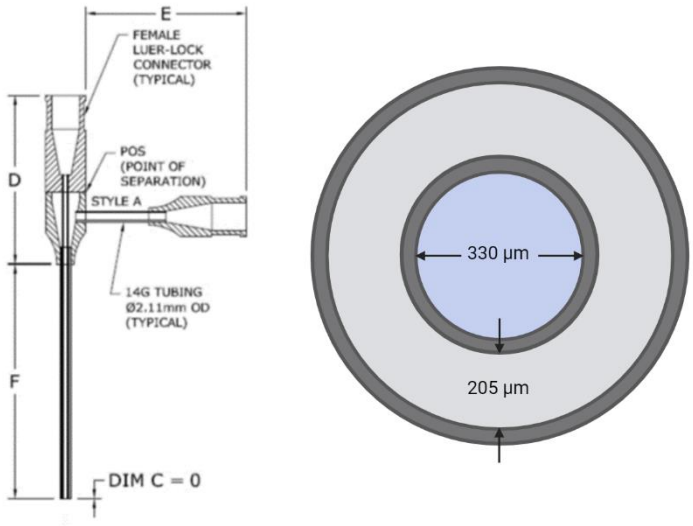

Fig. 22. Diagram of entire spinneret (SKE Research Equipment) and cross-section (blue = bore fluid, gray = dope solution).

MilliQ water was used for both the bore fluid and external nonsolvent bath due to its property as a strong coagulant and usage in the nonsolvent bath for flat sheet film synthesis. However, knowing that the polymer dope solutions were relatively nonviscous, we elected not to use ice cold conditions due to its effect of slowing solvent-nonsolvent exchange rate.

To determine the optimal air gap length, we aimed to strike a balance between sufficient coagulation time in air and gravitational/elongational forces. We performed preliminary tests from a 0 in (wet spinning) air gap to 5 in. Following these tests, we selected a 2 in air gap. We chose to have a takeup rate of 0 cm/min as to not impose additional elongational forces on the nascent fiber.

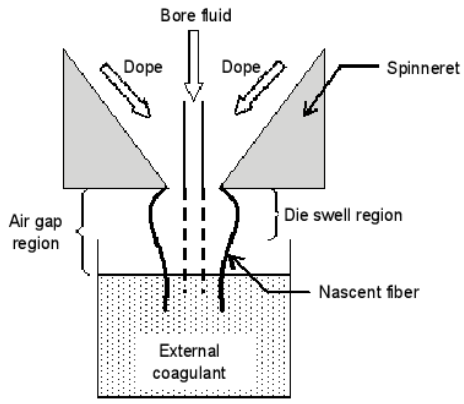

Figure 23. Illustration of die swell effect during dry-jet wet spinning (Bolong, 2017).

We also performed preliminary tests to assess fiber integrity at different flow rates. At low flow rates, fibers would not retain the cylindrical geometry. At high flow rates, fibers underwent the die swell effect, in which the polymer solution deforms and swells upon exiting the spinneret (Fig. 23). Following these tests, we selected a dope flow rate of 4.1 mL/min (average velocity = 200.7 cm/s) and bore flow rate of 10.3 mL/min (average velocity = 28.8 cm/s). All parameters are summarized in Table 4.

Fixed spinning parameters	**Conditions**
Spinneret dimensions	18G outer needle (OD = 1240 µm, ID = 840 µm), 23G inner needle (OD = 635 µm, ID = 330 µm)
Dope flow rate (mL/min)	4.1
Bore flow rate (mL/min)	10.3
Bore fluid composition	Water
External nonsolvent bath composition	Water
Bore and bath temperature (ºC)	25
Air gap (in)	2
Takeup rate (cm/min)	Free falling

Table 4. Fixed parameters for hollow fiber spinning.

3.2.4 Scanning Electron Microscopy

Scanning electron microscope (SEM) images were obtained using a SNE-3200M scanning electron microscope (NanoImages, LLC). Hollow fibers were dried thoroughly and sputter coated

with gold prior to imaging. The accelerating voltage was set to 5 kV, the detection mode was set to scanning electron mode, and the magnification ranged from 30X to 1000X.

3.3 Results and Discussion

3.3.1 Mathematical Analysis of Spinning Stresses

Since the formation of HF membranes is more complex than that of flat sheet membranes, we seek to understand how viscosity-dependent stresses influence the membrane morphology. If we consider the annular section F through which the polymer dope solution flows, we note that the length (5 mm) to annular thickness (205 µm) ratio exceeds 10 **(**Fig. 22**)**. Thus, we can assume that the flow is fully developed. Furthermore, we note that the spinneret has a flow angle of 90º, and that there is no take-up roller causing additional elongational stress. If we assume that the solution can be approximated as Newtonian, we can harness the following equations derived by S. J. Shilton to give a mathematical estimate of the shear rate $\dot{\gamma}$ and shear stress T as a function of radial position r across the annulus (Shilton, 1998):

$$\dot{\gamma} = \left(\frac{8Q}{\pi} \frac{1}{\frac{(R_2^2 - R_1^2)^2}{\ln\left(\frac{R_2}{R_1}\right)} - (R_2^4 - R_1^4)} \right) \times \left(\frac{r}{2} + \frac{(R_2^2 - R_1^2)^2}{4r \ln\left(\frac{R_1}{R_2}\right)} \right)$$

$$T = \eta\dot{\gamma}$$

where Q is the flow rate, R_1 is the inner radius, R_2 is the outer radius, and η is the dynamic viscosity of the dope solution. Per our system, we used $Q = 6.833 \times 10^{-8}\ \frac{m^3}{s}$, $R_1 = 635 \times 10^{-6}\ m$, and $R_2 = 840 \times 10^{-6}\ m$. We ran the function for $\eta = 0.5, 1.0, 1.5\ Pa \cdot s$ as they roughly encompassed the range of expected viscosities of our solutions. 16 wt% PSF in NMP was estimated to be

between 1 and 1.5 Pa·s (Kulichikhin, 2020; Anokhina, 2021). 16 wt% CA in an acetone-based mixed solvent was estimated to be around 0.4 Pa·s (Tungprapa, 2007).

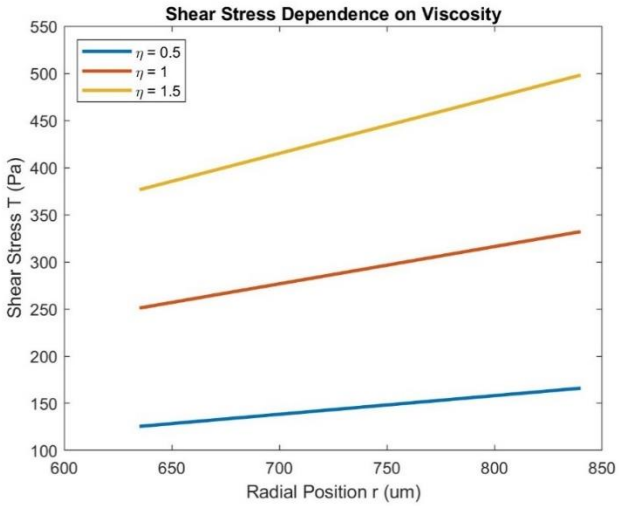

Figure 24. Shear stress vs. radial position for a range of viscosities.

Fig. 24 depicts the mathematical estimate of the sheer stress across the annulus, confined to the radial positions in which polymer flow is present. For each viscosity condition, we observe a mostly linear trajectory, with the greatest shear stress being experienced at the outside edge of the annulus and least stress at the interior. Increasing the viscosity linearly increases the shear stress at all positions along the annulus. From this model, we can see that at higher viscosities, the stress experienced at the external edge of the flow will be much higher than the stress at the inner edge. However, at our working range of viscosities, shear stress remains relatively low along the entire flow profile. In this low shear rate range, we may observe improved molecular orientation and chain packing with increased shear rate (Chung, 2000). We do not cross the threshold in which too high of a shear rate causes shear thinning of the polymer dope solution, creating a defective skin structure. Thus, we expect an enhancement of membrane selectivity with higher viscosity.

3.3.2 Cellulose Acetate Hollow Fibers

Given the success of the mixed solvent CA flat sheet membrane, we first attempted hollow fiber spinning with the same solution: 14.09 wt% cellulose acetate, 45.77 wt% dioxane, 17.61 wt% acetone, 8.45 wt% acetic acid, and 14.09 wt% methanol. However, we were only able to generate structures with defective morphology due to the low viscosity and subsequent low rate of solvent-

nonsolvent exchange. The cellulose acetate detachment times from Fig. 21 shows that detachment occurs after more than 160 s at every concentration of cellulose acetate tested. Since the nascent fiber only has 2 in of free fall space prior to entering the external nonsolvent bath, it must solidify very quickly to retain its shape and break the surface tension of the bath.

At bore fluid rate = 1.7 mL/min and dope solution rate 0.67 mL/min, we observed the formation of polymer "droplets". The pendant drop consists of both polymer and bore fluid and has not solidified enough to overcome the surface tension. Gravity is the primary force driving the polymer to fall from the spinneret. At this low bore and dope flow rate, we obtain half-spherical polymer pellets with a hole at the center (Fig. 26).

Fig. 25. Formation of CA "droplets". Bore rate = 1.7 mL/min, dope rate = 0.67 mL/min.

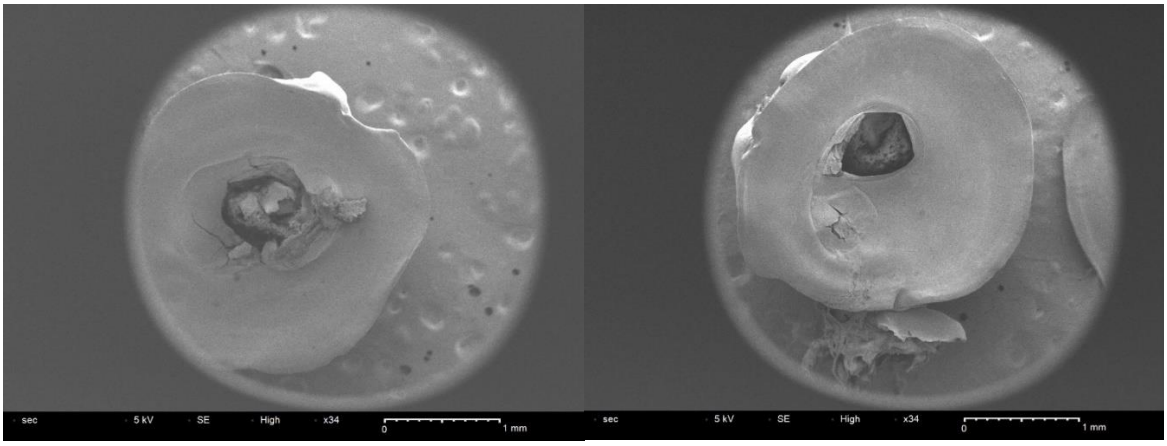

Fig. 26. SEM images of CA "droplets". Bore rate = 1.7 mL/min, dope rate = 0.67 mL/min.

Examining the morphology of these CA pellets, we measure the inner diameter to be around 0.6 mm and the outer diameter to be 2.5 mm. Therefore, the wall thickness is around 1.9 mm, far exceeding the dimensions of the spinneret nozzle (annular thickness = 0.205 mm). Such a polymer shape formed due to the slow demixing rate, in which bore fluid at the center of the

dope solution did not solidify the polymer, rather causing the dope to balloon out and form a pendant drop shape. The thick walls of the pellets are very dense with little distinguishing morphology, but the interior of the pellets have a highly sponge-like morphology. The spongey interior is indicative of very delayed demixing. Despite the usage of water, which is known to be a strong nonsolvent, the slow exchange of solvent and nonsolvent results in a sponge-like membrane interior.

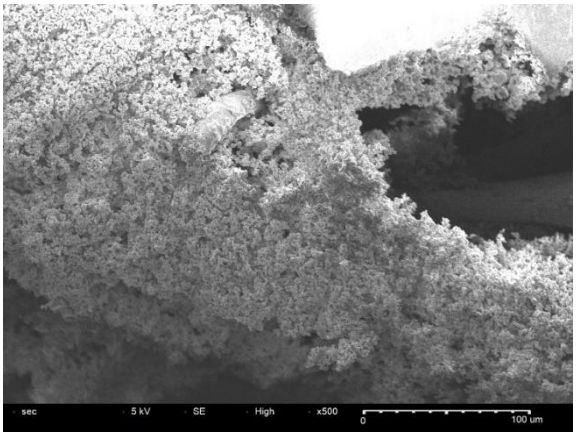

Figure 27. SEM image of spongey CA droplet interior. Bore rate = 1.7 mL/min, dope rate = 0.67 mL/min.

We next tested higher flow rates, with bore fluid rate = 4.1 mL/min and dope solution rate = 10.3 mL/min. Our rationale was that the higher flow rate and volume of polymer would overwhelm the surface tension causing the formation of the pendant droplet. While we were able to synthesize a continuous string of polymer, the structure remained defective. At the higher flow rate, the polymer had insufficient time to precipitate out of solution before landing in the nonsolvent bath. Thus, while we resolved the droplet problem and had a continuous polymer fiber, the nascent fiber had not solidified and remained in a semi-liquid phase after reaching the bath. The nascent fiber was therefore unable to penetrate the surface tension of the water bath, resulting in deformation of fibers. The nascent fiber then completed the majority of the solvent-nonsolvent exchange while floating at the surface of the nonsolvent bath.

Fig. 28. Formation of CA HFs. Bore rate = 10.3 mL/min, dope rate = 4.1 mL/min.

Fig. 29 shows the general appearance of the synthesized fibers. They exhibit irregular, non-circular cross sections due to the deformation of the polymer floating atop the nonsolvent bath (Fig. 29a). If we approximate the cross section as an ellipse, it has dimensions of 2 mm x 0.5 mm. In addition to the deformed elliptical shape, we also observed fibers with nonuniform flaky cross sections (Fig. 29b). Though seemingly inconsistent with the dense spongy structure CA typically generates due to delayed demixing, these flaky layers are caused by gravitational/elongational stress. As the soft nascent fiber falls through the air gap, slow solvent-nonsolvent exchange is occurring. However, the low structural integrity of the fiber causes stretching during the slow precipitation, with bore fluid filling the gaps, forming a disorganized, layered cross section.

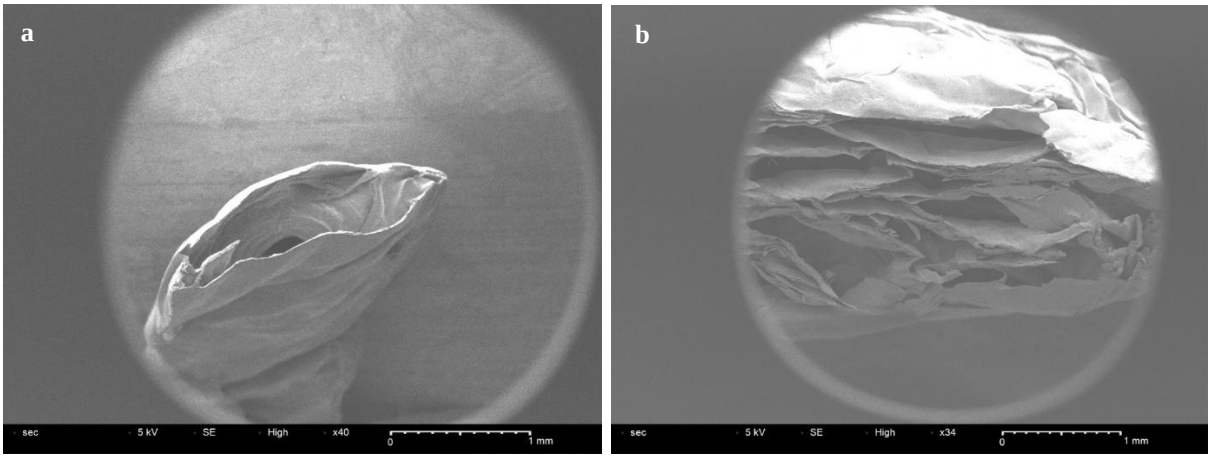

Fig. 29. SEM images of defective CA HFs. Bore rate = 10.3 mL/min, dope rate = 4.1 mL/min.

The walls of the synthesized fibers resemble that of the flat sheet membranes. From Fig. 30, the wall thickness of the HF membrane varies between 10-20 μm, while the wall thickness of the flat sheet membrane is more uniform at ~15 μm. However, we do not observe the clear skin layer and support layer in the HF membrane wall. Fig. 30a shows that the wall contains many irregular structures and gaps, likely due to the bore fluid and nonsolvent bath permeating the dope solution unevenly.

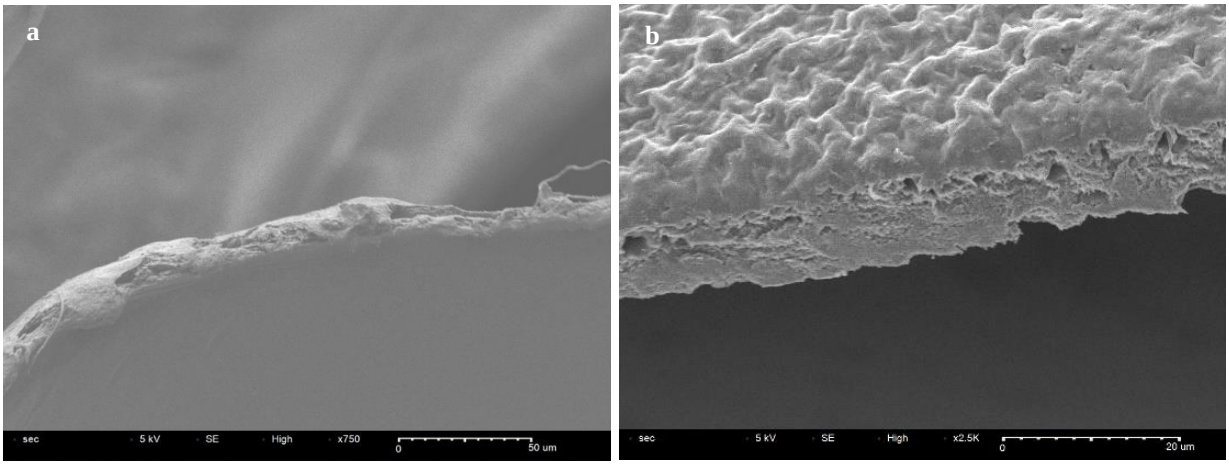

Fig. 30. SEM images of a) CA HF membrane (bore rate = 10.3 mL/min, dope rate = 4.1 mL/min) and b) CA flat sheet membrane. Both synthesized with mixed solvents.

3.3.3 Polysulfone Hollow Fibers

Following CA, we chose to evaluate PSF in NMP as a potential candidate due to the solvent-nonsolvent exchange data obtained in section 2.3.8. For PSF and CA polymer dope solutions of similar concentrations, PSF demonstrated a 11.7X faster detachment time and a 3.6X faster time to opacity. Therefore, we synthesized PSF HFs under the same conditions of bore fluid rate = 4.1 mL/min and dope solution rate = 10.3 mL/min.

Using a 16 wt% PSF in NMP dope solution, we were able to generate HFs with the characteristic cylindrical morphology (Fig. 31). Though the cross sections were not perfectly circular, they were vastly improved from the CA fibers with an approximate radius of 350 µm. This radius is aligned with our expectations for the size of a HF synthesized with a 23G needle within a 18G needle. The dope solution passes through an annular

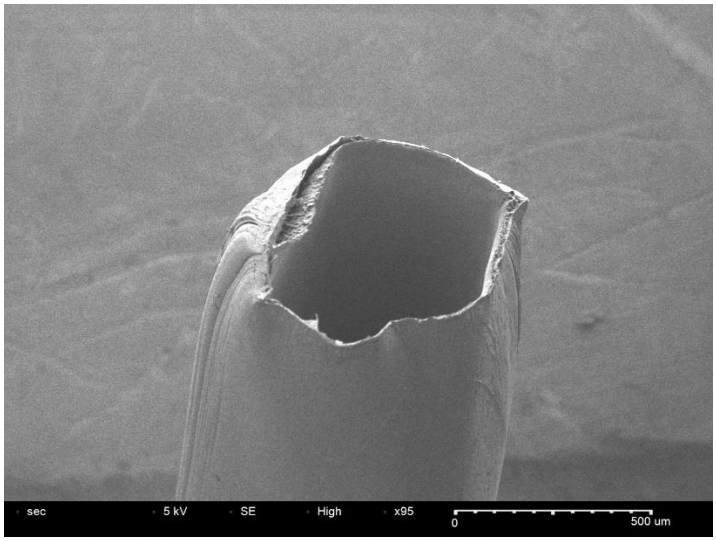

Figure 31. SEM image of PSF HFs synthesized from 16 wt% PSF in NMP. Bore rate = 10.3 mL/min, dope rate = 4.1 mL/min.

space of width 205 µm (840 µm – 635 µm). Thus, accounting for the loss of volume from the polymer/solvent system of the dope solution that occurs during demixing, we expect a diameter of 600 – 700 µm with a thin membrane wall on the order of the 10s of µm.

Examining the membrane wall, we do indeed observe a wall thickness of approximately 25 µm (Fig. 32a). There is a dense skin layer on both the interior and exterior of the HF, which form during contact with the bore fluid and external nonsolvent bath respectively. Large macrovoids are located between the two skin layers, with channels up to 10 µm in width. We also observe in a different section of the HF wall that delamination is occurring, in which the interior and exterior layers of the HF appear to be separating (Fig 32b). This phenomenon can occur when the solvent/nonsolvent diffusion rate and membrane shrinkage rate differs at the inner and outer interface. In our system, delamination likely took place because of phase inversion happening at different rates for the inner and outer surfaces of the HF. Since the PSF dope solution is known to have near instantaneous demixing, contact of the inner layer with the bore fluid initiated demixing and shrinking of the inner layer. However, once the HF is immersed in the external bath, the large volume of nonsolvent accelerates demixing for the outer layer. Compared to the mutual diffusion initiated by the thin stream of bore fluid, the demixing at the outer layer occurs much faster, causing the outer layer to form large water-holding macrovoids that exist at the interface between the inner and outer layers. Fig. 32a shows that at the inner layer, there are smaller macrovoids underneath the inner dense skin layer that transition into the large channels within the membrane. However, there are no small macrovoids immediately under the outer dense skin layer; the skin layer transitions straight into the large channeled structures. These observations provide additional evidence that the outer layer undergoes a higher rate of solvent-nonsolvent exchange than the inner layer, resulting in large nonsolvent-filled macrovoids that contribute to delamination.

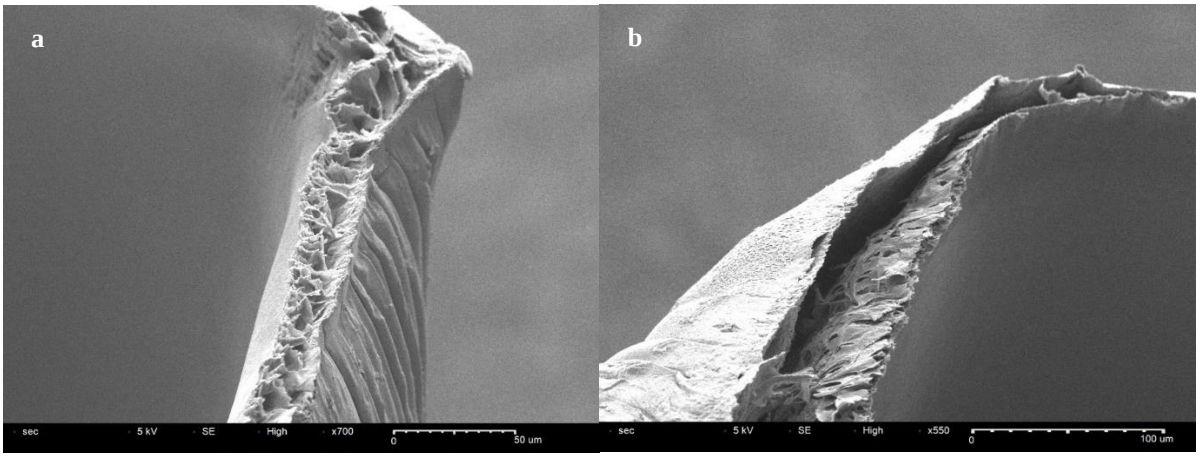

Figure 32. SEM images of PSF HFs synthesized from 16 wt% PSF in NMP depicting a) a nondelaminated wall and b) a delaminated wall. Bore rate = 10.3 mL/min, dope rate = 4.1 mL/min.

3.3.4 Polyethersulfone Hollow Fibers

Finally, we synthesized HFs with 16 wt% PES in NMP solution. With PES, we generated HFs with a uniform and circular cross section (Fig. 33). The somewhat oval shape is caused by the pressure of the razor when cutting a sample, but the HFs are otherwise circular with a radius of approximately 300 µm. As previously determined, we expect a diameter of 600 – 700 µm with a thin membrane wall on the order of the 10s of µm. From Fig. 34, the PES HFs have a wall thickness of 50 µm. Thus, the overall bulk structure of the HF falls within our expectations.

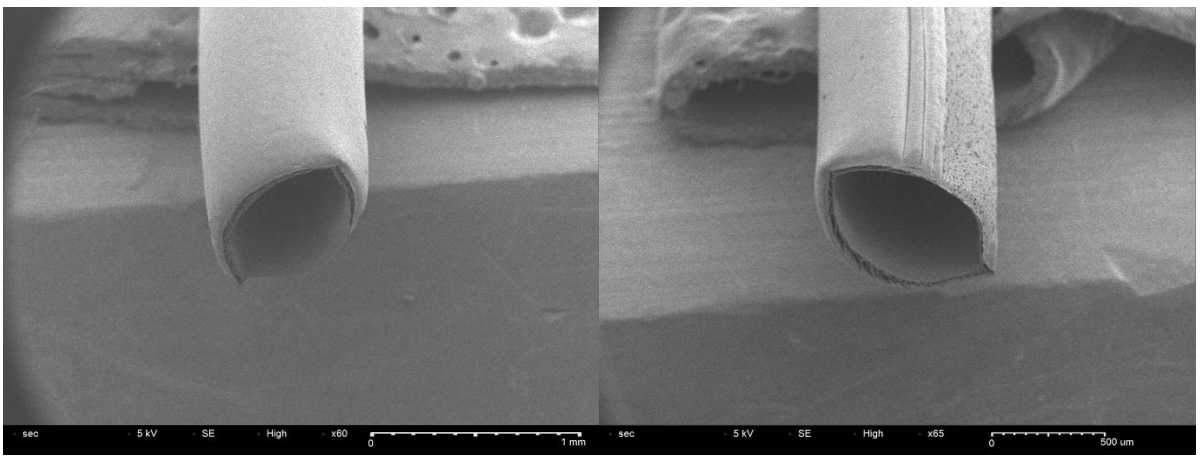

Fig. 33. SEM image of PES HFs synthesized from 16 wt% PES in NMP. Bore rate = 10.3 mL/min, dope rate = 4.1 mL/min.

Examining the specific wall structure, we observe an unusual multilayer morphology that occurs in a few sections of the HFs. From Fig. 34a, a thin layer has formed between the dense

outer skin layer and the large macrovoids. Within this thin layer appears to be another dense skin layer with a small supporting structure. Though the mechanism behind the formation of this intermediate layer is not definitive, there are a few possibilities. The intermediate layer could be the polymer-lean support layer for the outer skin layer that formed after the nascent fiber contacted the external nonsolvent bath. The subsequent formation of large, water-filled macrovoids may have induced slight delamination, giving the appearance of a third intermediate layer. Another study with PES HFs theorized that when using a weaker coagulant for bore fluid, a very small amount of bore fluid may permeate through the dense inner skin layer (Feng, 2021). This then forms a mixture of bore fluid and uncoagulated dope solution within the nascent fiber. Then, when the HF drops into the external nonsolvent bath, the section within the fiber with the bore fluid/dope solution mixture precipitates into an intermediate layer. It is uncertain if such an effect can also take place if a strong coagulant such as water is used for the bore fluid. However, it is likely that the phase separation and delamination kinetics are key factors in the formation of multiple layers within the HF.

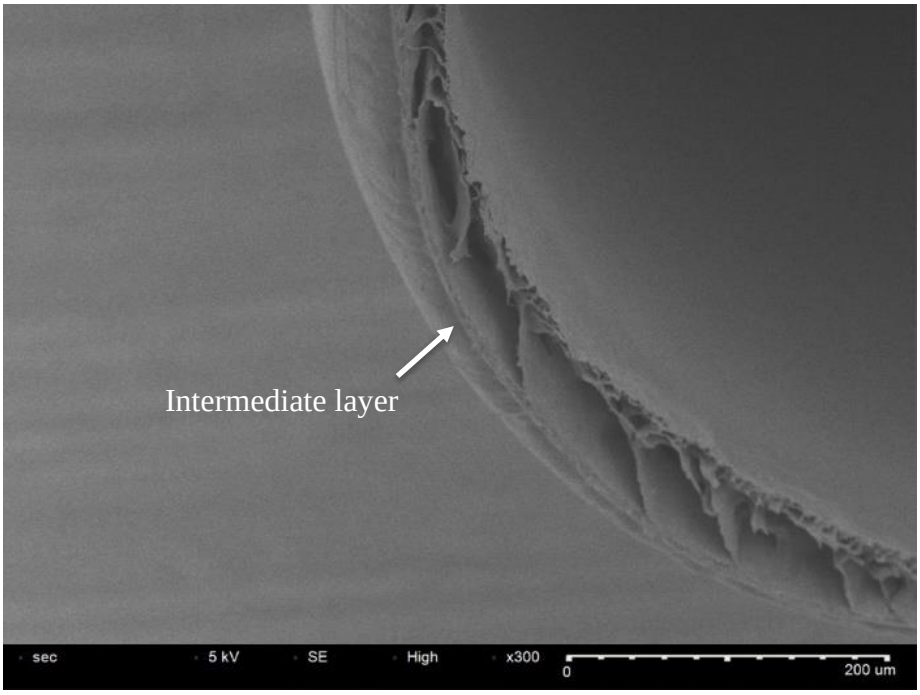

Fig. 34. Close-up SEM image of PES HF synthesized from 16 wt% PES in NMP, highlighting the intermediate third layer formed within the wall.

The unusual morphology with the intermediate layer was not observed for all samples. In Figs. 35 and 36, we notice smaller channeled macrovoids forming a support layer adjacent to the inner skin layer. The small macrovoids transition rapidly to the very large, layered structures that lie adjacent to the outer skin layer. Like for the PSF HFs, these large, layered structures form after near instantaneous demixing in the external nonsolvent bath and fill with nonsolvent. Though the layers are nonuniform and have voids of up to 40 μm, we do not observe as much delamination for PES HFs. Fig. 36a shows a sample with some delamination between the inner and outer layers, causing a breakdown in the structural integrity of the membrane in which the layers appear pinched together.

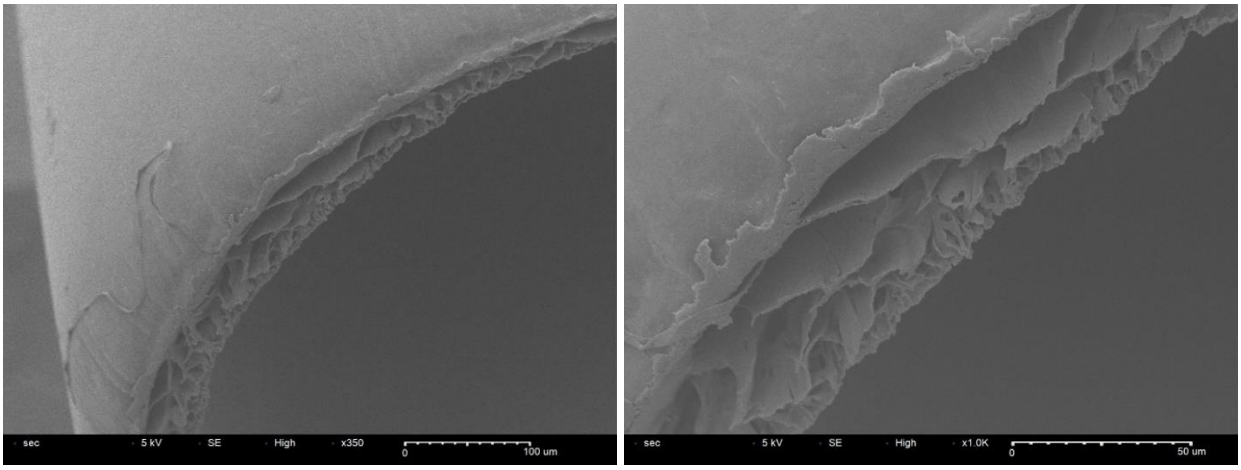

Fig. 35. SEM images of PES HF synthesized from 16 wt% PES in NMP.

Another consideration is the filtration potential of PES HFs, since they appear structurally feasible for dialysate filtration. Flat sheet experiments for PES revealed poor selectivity for urea over glucose. At 16 wt% PES, we observed good overall flux through the membrane but a low urea to glucose permeation ratio. Increasing the concentration decreased the flux without improving selectivity. Though further testing is necessary in a filtration cell for confirmation, there are a few key differences with HF membranes that may improve selectivity. HFs are formed by exposing two sides of the dope solution to nonsolvent as opposed to one side as is standard for flat

sheet membranes. This means that two dense skin layers typically form, providing two layers through which molecular separation can occur. In Fig. 36, the inner skin layer is substantially thinner than the outer skin layer. This may be caused by the evaporation time as the nascent fiber falls through the air gap, in which nonsolvent evaporates from the surface of the dope solution and a higher concentration of polymer accumulates at the air-dope solution interface due to capillary forces. A thicker skin layer is then formed upon immersion in the nonsolvent. A second reason is that the mild shear stress near the exterior edge of the HF was found in section 3.3.1 to be within the range for improved chain packing. Thus, the increased shear stress at the outer edge compared to the inner edge may result in a denser and thicker polymer layer forming at the exterior side of the HF. The outer skin layer may therefore provide improved molecular separation performance, with the molecular reorientation of shear stress having a similar chain packing effect in HF synthesis to thermal annealing in flat sheet membrane synthesis.

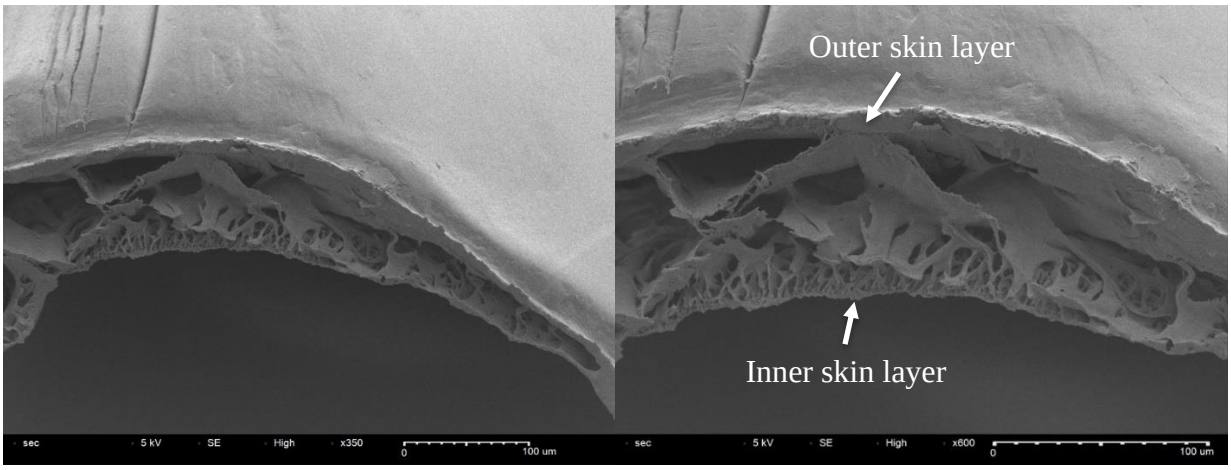

Fig. 36. SEM images of PES HF synthesized from 16 wt% PES in NMP with slight delamination and highlighting the skin layers.

3.4 Conclusions and Future Directions

In this chapter, we discussed the selection of parameters for HF spinning, performed analysis of the HF spinning process using a mathematical model, synthesized HFs with a wide range of morphologies, and critically examined the morphologies of each synthesized HF. We

narrowed the spinning parameters down to a spinneret with 18G outer needle and 23G inner needle, dope flow rate of 4.1 mL/min, bore flow rate of 10.3 mL/min, room temperature water as the bore fluid and nonsolvent bath, 2 in air gap, and no takeup rate (free falling). We examined the system under a mathematical model and determined that the shear forces on our dope solution would have a chain packing effect and improve selectivity. We then synthesized CA, PSF, and PES HFs using the predetermined parameters. We found that directly converting the mixed solvent CA procedure from the flat sheet membrane configuration is impractical due to slow demixing of solvent and nonsolvent. We analyzed the defective CA HFs, finding a spongey interior indicative of delayed demixing. PSF HFs had improved morphology, with a distinctive hollow cylindrical structure. The dimensions of the HFs were within our expectations, and the thin membrane wall was similar in thickness to the flat sheet PSF membranes. However, the PSF HFs had noticeable delamination due to more rapid demixing occurring at the exterior sides of the membranes. PES membranes exhibited the most regular morphology, with well-formed fibers and uniform walls. We inquired into unusual intermediate layer formation for PES HFs and assessed their suitability for urea/glucose filtration. We discussed the key differences that may confer advantageous properties to PES HFs over flat sheet membranes, such as the presence of additional skin layers for filtration and the chain packing effect of shear forces. In addition, PES previously demonstrated improved wettability compared to PSF. This is consistent with the increased concentration of sulfone groups per PES unit. Thus, PES may have greater suitability in an aqueous environment with proteins present, as less protein fouling is likely to occur on PES compared to PSF.

Immediate future directions include setting up a filtration module to test the PES HFs on dialysate solution. We can also consider alternative methods to make CA a more suitable candidate for HF spinning. These include modulating the viscosity using temperature or changing the

composition of the mixed solvents to be more miscible with water and thus promoting the rate of demixing. In the future, we can also inquire into HFs spun with spinnerets of different dimensions and the effect of thermal annealing on HF membranes. We may also even consider incorporating channels such as aquaporins into the polymer matrix. Ultimately, the HF characterization results presented in this chapter will guide further development of HFs for the separation of urea and glucose in dialysate.

Chapter 4: Overall Conclusions

The objective of this thesis was to generate and characterize polymeric materials for separation of urea and glucose in dialysate. We specifically evaluated flat sheet and hollow fiber membranes, critically assessing the parameters involved in their synthesis and the mechanism of material formation.

We synthesized a flat film membrane using a dope solution of cellulose acetate in mixed solvent (dioxane, acetone, acetic acid, and methanol), ice cold synthesis conditions, and 1 h of thermal annealing at 65ºC. This specific procedure allowed us to generate a membrane with high flux performance—filtration of 14 g of urea in 6 h—and high separation performance, with a urea to glucose permeation ratio of over 30. To facilitate the transition to hollow fiber synthesis, we analyzed the material properties of different flat sheet membranes to further understand the thermodynamic and kinetic mechanisms that drive their formation.

We then synthesized and analyzed the morphology of hollow fibers with different dope solution compositions. Following the flat sheet material characterization experiments, we probed into the specific mechanisms that resulted in the observed hollow fiber morphologies and evaluated their suitability for filtration applications. We found that PES hollow fiber membranes showed the most potential, highlighting specific elements (i.e. two skin layers, shear stress induced polymer reorientation) of hollow fiber synthesis that differentiate hollow fiber membranes from flat sheet membranes.

Our ultimate goal is the development of high performing hollow fibers which can be incorporated into a portable dialysis system alongside the established photoelectrochemical urea decomposition system. Globally, this innovation has potential to reduce ESRD mortality by improving patient adherence to dialysis and broadening access to treatment, especially in

locations without convenient access to dialysis clinics. Economically, it would remove the cost of high volumes (120 L per session) of fluid needed to generate dialysate. Such an innovation would also relieve some of the burden off hospitals with a shortage of dialysis technicians and allow for reallocation of funding and personnel. Environmentally, the innovation will save thousands of liters of water per patient. Socially, the device will allow greater patient autonomy and thus reduce stigma around dialysis. We hope for a future in which dialysis patients can spend more time engaging with family, friends, and the community to lead personally fulfilling lives.

References

Abbasi, M. A. (2010). End-stage renal disease. *BMJ Clinical Evidence*.

Ahmad, A. O. (2019). Hollow fiber (HF) membrane fabrication: A review on the effects of solution spinning conditions on morphology and performance. *Journal of Industrial and Engineering Chemistry*, 35-50.

Ali, N. H. (2012). Preparation and characterization of asymmetric ultrafiltration membrane for effective recovery of proteases from surimi wash water. *Frontiers of Chemical Science and Engineering*, 184-191.

Anokhina, T. R. (2021). Express Method of Preparation of Hollow Fiber Membrane Samples for Spinning Solution Optimization: Polysulfone as Example. *Membranes*.

Arora, P. (2021, April 2). *Chronic Kidney Disease (CKD)*. From Medscape.

Baker, R. (1999). *Membrane technology and applications.* New York: McGraw-Hill.

Baura, G. (2021). *Medical device technologies: A systems based overview using engineering standards (Second ed.).* Academic Press.

Blagg, C. (2007). The Early History of Dialysis for Chronic Renal Failure in the United States. *American Journal of Kidney Diseases*, 482-496.

Bleyer, A., Hartman, J., Brannon, P., Reeves-Daniel, A., Satko, S., & Russell, G. (2006). Characteristics of sudden death in hemodialysis patients. *Kidney International*, 2268-2273.

Bolong, N. I. (2017). Effect of Jet Stretch in the Fabrication of Polyethersulfone Hollow Fiber Spinning for Water Separation. *Journal of Applied Membrane Science & Technology*.

Centers for Disease Control and Prevention. (2021, March 4). *Chronic Kidney Disease in the United States, 2021*.

Cerqueira, D., Soares, C., Silva, V., Magalhães, J., Barcelos, I., Duarte, M., . . . Oliveira, E. (2014). A Predictive Model of Progression of CKD to ESRD in a Predialysis Pediatric Interdisciplinary Program. *Clin J Am Soc Nephrol 9*, 728-735.

Chakrabarty, B. C. (2008). Preparation, characterization and performance studies of polysulfone membranes using PVP as an additive. *Journal of Membrane Science*, 36-47.

Chang, Y. S. (2008). Preparation of poly(vinylidene fluoride) microfiltration membrane with uniform surface-copolymerized poly(ethylene glycol) methacrylate and improvement of blood compatibility. *Journal of Membrane Science*, 165-174.

Chertow, G. L. (2010). In-center hemodialysis six times per week versus three times per week. *N Engl J Med*, 2287-2300.

Chung, T. L. (2000). The effect of shear rates on gas separation performance of 6FDA-durene polyimide hollow fibers. *Journal of Membrane Science*, 55-66.

Claudio Ronco, L. F. (2007). The Vicenza wearable artificial kidney for peritoneal dialysis (ViWAK PD). *Blood Purif.*

Cockwell, P., & Fisher, L. (2020). The global burden of chronic kidney disease. *The Lancet*, 622-644.

Çulfaz, P. R. (2010). Microstructured hollow fibers for ultrafiltration. *Journal of Membrane Science*, 32-41.

Daugirdas, J. G. (2013). Effect of frequent hemodialysis on residual kidney function. *Kidney Int.*, 949-58.

Duarte, A. C. (2006). Cellulose acetate reverse osmosis membranes: Optimization of the composition. *Journal of Applied Polymer Science*, 4052-4058.

El-Gendi, A. A. (2007). Preparation and evaluation of flat membranes for phenols separation. *Desalination*, 226-237.

Feng, Y. W. (2021). Delamination of single layer hollow fiber membranes induced by bi-directional phase separation. *Journal of Membrane Science*.

Fornazier, M. d. (2021). Additives Incorporated in Cellulose Acetate Membranes to Improve Its Performance as a Barrier in Periodontal Treatment. *Frontiers in Dental Medicine*.

FreePurity. (n.d.). *Comparison Between Micro-Filtration, Ultra-Filtration and Nano-Filtration vs. Reverse Osmosis Purification of Drinking Water*. From https://www.freepurity.com/blogs/resources/micro-ultra-nano-filtration-vs-reverse-osmosis-whats-the-difference

Giwa, A. C. (2017). Nanoporous hollow fiber polyethersulfone membranes for the removal of residual contaminants from treated wastewater effluent: Functional and molecular implications. *Separation and Purification Technology*, 20-31.

Gwak, G. H. (2018). *Membrane-Based Salinity Gradient Processes for Water Treatment and Power Generation.* Elsevier.

Han, M. N. (2002). Thermodynamic and rheological variation in polysulfone solution by PVP and its effect in the preparation of phase inversion membrane. *Journal of Membrane Science*, 55-61.

Holda, A. V. (2014). Integrally skinned PSf-based SRNF-membranes prepared via phase inversion—Part B: Influence of low molecular weight additives. *Journal of Membrane Science*, 499-511.

Holda, A. V. (2015). Understanding and guiding the phase inversion process for synthesis of solvent resistant nanofiltration membranes. *Journal of Applied Polymer Science*.

Huang, H. Y. (2006). Filtration characteristics of polysulfone membrane filters. *Journal of Aerosol Science*, 1198-1208.

Idris, A. M. (2017). Effects of Phase Separation Behavior on Morphology and Performance of Polycarbonate Membranes. *Membranes*.

Imemflo. (2023, June 8). *Difference between hollow fiber and flat sheet membrane*. From https://www.imemflo.com/difference-between-hollow-fiber-and-flat-sheet-membrane/#:~:text=Hollow%20fiber%20membranes%20offer%20a,collected%20from%20the%20other%20side.

Ji, H. L. (2023). Advances in Enhancing Hemocompatibility of Hemodialysis Hollow-Fiber Membranes. *Advanced Fiber Materials*, 1198-1240.

Kassim Shaari, N. A. (2017). Thin Film Composite Membranes: Mechanical and Antifouling Properties. *MATEC Web of Conferences.*

Khayet, M. (2003). The effects of air gap length on the internal and external morphology of hollow fiber membranes. *Chemical Engineering Science*, 3091-3104.

Kim, N. B. (2023). Application of Hollow Fiber Membrane for the Separation of Carbon Dioxide from Atmospheric Air and Assessment of Its Distribution Pattern in a Greenhouse. *Atmosphere*.

Kohlova, M. A.-S. (2019). The biocompatibility and bioactivity of hemodialysis membranes: Their impact in end-stage renal disease. *J Artif Organs*.

Kulichikhin, V. M. (2020). Rheology of polysulfone-N-methylpyrrolidone solutions used in the technology of lithium-ion batteries. *Applied Rheology*, 102-106.

Lau, H. L. (2022). State-of-the-Art Organic- and Inorganic-Based Hollow Fiber Membranes in Liquid and Gas Applications: Looking Back and Beyond. *Membranes*.

Madaeni, S. M. (2011). Preparation and characterization of asymmetric polysulfone membrane for separation of oxygen and nitrogen gases. *Journal of Applied Pol2011ymer Science,* 2157-2167.

Matovinovic, M. (2009). Pathophysiology and Classification of Kidney Diseases. *EJIFCC,* 2-11.

Mayo Clinic. (n.d.). *End-stage renal disease*. From Mayo Clinic.

Minoli, D. (2005). *Nanotechnology Applications to Telecommunications and Networking.* Wiley-Interscience 1 edition.

Peng, N. W. (2012). Evolution of polymeric hollow fibers as sustainable technologies: Past, present, and future. *Progress in Polymer Science,* 1401-1424.

Perl, J. (2014). Kidney Transplant Failure: Failing Kidneys, Failing Care? *Clin J Am Soc Nephrol*, 1153-1155.

Ronco, C. C. (2018). Haemodialysis membranes. *Nat Rev Nephrol.*, 394-410.

Ronco, C. C. (2018). Haemodialysis membranes. *Nat Rev Nephrol.*

Ruggiero, R. C. (2015). Study of in vitro degradation of cellulose acetate membranes modified and incorporated with tetracycline for use as an adjuvant in periodontal reconstitution. *Industrial Crops and Products,* 2-6.

Rwei, S.-P. (2001). Formation of hollow fibers in the melt-spinning process. *Journal of Applied Polymer Science*, 2896-2902.

Saleh, N. A. (2009). Effect of alcohol as additives on the morphology and separation performance of polyethersulfone (PES) hollow fiber ultrafiltration membranes. *Engineering and Technology Journal*, 1263-1273.

Salijoughi, E. M. (2009). Cellulose acetate (CA)/polyvinylpyrrolidone (PVP) blend asymmetric membranes: Preparation, morphology and performance. *Desalination,* 850-854.

Saran, R., R. B., Abbott, K. C., Bragg-Gresham, J., Chen, X., Gipson, D., . . . Repeck, K. (2020). U.S. Renal Data System 2019 Annual Data Report: Epidemiology of Kidney Disease in the United States. *AJKD*, A6-A7.

Setiawan, L. S. (2012). Explorations of delamination and irregular structure in poly(amide-imide)-polyethersulfone dual layer hollow fiber membranes. *Journal of Membrane Science*, 73-84.

Sewerin, T. E. (2021). Advances and Applications of Hollow Fiber Nanofiltration Membranes: A Review. *Membranes*.

Shaikh, H., Hashmi, M., & Aeddula, N. (2023). Anemia of Chronic Renal Disease. *StatPearls [Internet]*.

Shao, G. Z. (2019). TiO2 Nanowires Based System for Urea Photodecomposition and Dialysate Regeneration. *ACS Appl. Nano Mater.*, 6116-6123.

Shilton, S. (1998). Flow profile induced in spinneret during hollow fiber membrane spinning. *Journal of Applied Polymer Science*.

Soroko, I. L. (2011). The effect of membrane formation parameters on te performance of polyimide membranes for organic solvent nanofiltration (OSN): Park A. Effect of polymer/solvent/non-solvent system choice. *Journal of Membrane Science*, 152-162.

Stein, W. (1986). *Transport and Diffusion across Cell Membranes.* Academic Press Inc.

Strathmann, H. K. (1977). The Formation Mechanism of Phase Inversion Membranes. *Desalination*, 241-255.

Toh, Y. L. (2007). Polymeric membranes for nanofiltration in polar aprotic solvents. *Journal of Membrane Science*, 3-10.

Tungprapa, S. P. (2007). Electrospun cellulose acetate fibers: Effect of solvent system on morphology and fiber diameter. *Cellulose*, 563-575.

United States Renal Data System. (2018). *2018 USRDS annual data report: Epidemiology of kidney disease in the United States.* Bethesda, MD: National Institutes of Health, National Institute of Diabetes and Digestive and Kidney Diseases.

Van Gelder, M. J. (2020). Urea removal strategies for dialysate regeneration in a wearable artificial kidney. *Biomaterials*.

Vatanpour, V. P. (2022). Cellulose acetate in fabrication of polymeric membranes: A review. *Chemosphere (Oxford)*.

Widjojo, N. C. (2006). Thickness and Air Gap Dependence of Macrovoid Evolution in Phase-Inversion Asymmetric Hollow Fiber Membranes. *Ind. Eng. Chem. Res.*, 7618-7626.

Widjojo, N. C. (2010). Elimination of die swell and instability in hollow fiber spinning process of hyperbranched polyethersulfone (HPES) via novel spinneret designs and precise spinning conditions. *Chemical Engineering Journal*, 142-153.

Yin, J. Z. (2020). Highly selective oxidation of glucose to gluconic acid and glucaric acid in water catalyzed by an efficient synergistic photocatalytic system. *Catalysis Science & Technology*.